

# Simulation of self-assembled nanopatterns in binary alloys on the fcc(111) surface

Dissertation zur Erlangung des  
naturwissenschaftlichen Doktorgrades  
der Julius-Maximilians-Universität Würzburg

vorgelegt von  
Sebastian Weber  
aus Ochsenfurt

WÜRZBURG 2008

Eingereicht am 22. Februar 2008  
bei der Fakultät für Physik und Astronomie

1. Gutachter: Priv. Doz. Dr. M. Biehl  
2. Gutachter: Prof. Dr. W. Kinzel  
der Dissertation.

1. Prüfer: Prof. Dr. F. Assaad  
2. Prüfer: Prof. Dr. W. Kinzel  
3. Prüfer: Prof. Dr. J. Geurts  
im Promotionskolloquium.

Tag des Promotionskolloquiums: 20. Juni 2008

Doktorurkunde ausgehändigt am:

# Zusammenfassung

Diese Doktorarbeit beschäftigt sich mit der Untersuchung von heteroepitaktischem Kristallwachstum mit Hilfe von Monte Carlo Simulationen. Von besonderem Interesse ist hierbei der Einfluss des Gitterunterschieds zwischen den Adsorbatmaterialien und dem Substrat auf die Oberflächenstrukturen. Unter Verwendung eines gitterfreien Modells betrachten wir die erste Monolage des Adsorbats und untersuchen die entstehenden Nanostrukturen sowie deren Entwicklung während des Wachstums. Kapitel 1 gibt dazu eine kurze Einführung, welche die Rolle von Computersimulationen im Gebiet der modernen Festkörperphysik beschreibt.

Kapitel 2 widmet sich einigen technischen Grundlagen der Molekularstrahlepitaxie und deren theoretischen Behandlung. Bevor ein Modell für die Simulation erstellt werden kann, ist es notwendig einige Überlegungen über die einzelnen Prozesse anzustellen, welche beim epitaktischen Wachstum in Erscheinung treten. Zu diesem Zweck betrachten wir zunächst den experimentellen Aufbau und entnehmen die wichtigsten mikroskopischen Prozesse. Danach wird ein kurzer Überblick über die verschiedenen theoretischen Konzepte gegeben, die diese physikalischen Vorgänge beschreiben.

In Kapitel 3 wird anschließend das in den Simulationen verwendete Modell vorgestellt. Das Ziel dieser Arbeit ist die Untersuchung des Wachstums eines fcc Kristalls in die  $[111]$  Richtung. Um die Simulationszeiten in realisierbaren Grenzen zu halten, wird ein einfaches Paar-Potential, das Lennard-Jones Potential, mit kontinuierlichen Koordinaten verwendet, welche notwendig sind, um Effekte zu beschreiben, die ihren Ursprung in der atomaren Fehlanpassung im Kristall besitzen. Außerdem wird der detaillierte Algorithmus erläutert, welcher darauf basiert zunächst die Barriere eines jeden Diffusionsereignisses zu berechnen, um diese Barrieren dann in einem verwerfungsfreien Algorithmus zu verwenden.

Kapitel 4 beschäftigt sich mit der Simulation von Gleichgewichtskonfigurationen. Dabei wird der Einfluss verschiedener Parameter auf die entstehenden Strukturen in der ersten Monolage auf dem Substrat untersucht, welches vollständig mit zwei Adsorbatmaterialien bedeckt ist. Besonders die Konkurrenz zwischen Bindungsenergie und Verspannung führt zur Bildung äußerst interessanter Strukturen wie Inseln oder Streifen.

Im Anschluss werden in Kapitel 5 die Ergebnisse von Wachstumssimulatio-

nen präsentiert. Zu Beginn stellen wir das Modell vor, das den gitterfreien Monte Carlo Simulationen zu Grunde liegt. Da sich der numerische Aufwand in enormen Simulationszeiten niederschlägt, werden einige Vereinfachungen bei der Berechnung der Diffusionsbarrieren notwendig und aus diesem Grund werden dem bis dahin verwendeten Modell einige Elemente des sogenannten Ball and Spring Modells hinzugefügt. Der nächste Abschnitt widmet sich dann den Berechnungen der Energiebarrieren, bevor die Ergebnisse der Wachstumssimulationen vorgestellt werden. Dabei werden sowohl binäre Systeme mit nur einer Adsorbatsorte als auch ternäre Systeme mit zwei Adsorbatkomponenten untersucht. Abschließend wird ein Vergleich zu den Ergebnissen der Gleichgewichtssimulationen aus dem Kapitel vorher gezogen.

Kapitel 6 beinhaltet schließlich einige zusammenfassende Bemerkungen und bietet einen Ausblick auf mögliche weitere Untersuchungen.

# Abstract

In this PhD thesis, we study the heteroepitaxial crystal growth by means of Monte Carlo simulations. Of particular interest in this work is the influence of the lattice mismatch of the adsorbates relative to the substrate on surface structures. In the framework of an off-lattice model, we consider one monolayer of adsorbate and investigate the emerging nanopatterns in equilibrium and their formation during growth. In chapter 1, a brief introduction is given, which describes the role of computer simulations in the field of the physics of condensed matter.

Chapter 2 is devoted to some technical basics of experimental methods of molecular beam epitaxy and the theoretical description. Before a model for the simulation can be designed, it is necessary to make some considerations of the single processes which occur during epitaxial growth. For that purpose we look at an experimental setup and extract the main microscopic processes. Afterwards a brief overview of different theoretical concepts describing that physical procedures is given.

In chapter 3, the model used in the simulations is presented. The aim is to investigate the growth of an fcc crystal in the  $[111]$  direction. In order to keep the simulation times within a feasible limit a simple pair potential, the Lennard-Jones potential, with continuous particle positions is used, which are necessary to describe effects resulting from the atomic mismatch in the crystal. Furthermore the detailed algorithm is introduced which is based on the idea to calculate the barrier of each diffusion event and to use the barriers in a rejection-free method.

Chapter 4 is attended to the simulation of equilibrium. The influence of different parameters on the emerging structures in the first monolayer upon the surface, which is completely covered with two adsorbate materials, is studied. Especially the competition between binding energy and strain leads to very interesting pattern formations like islands or stripes.

In chapter 5 the results of growth simulations are presented. At first, we introduce a model in order to realize off-lattice Kinetic Monte Carlo simulations. Since the costs in simulation time are enormous, some simplifications in the calculation of diffusion barriers are necessary and therefore the previous model is supplemented with some elements from the so-called ball and spring model. The next point is devoted to the calculation of energy barriers followed by the presentation of the growth simulations. Binary systems with only one sort of adsorbate

are investigated as well as ternary systems with two different adsorbates. Finally, a comparison to the equilibrium simulations is drawn.

Chapter 6 contains some concluding remarks and gives an outlook to possible further investigations.

# Contents

<b>1</b>	<b>Introduction</b>	<b>9</b>
<b>2</b>	<b>Theoretical background</b>	<b>11</b>
2.1	Molecular beam epitaxy . . . . .	11
2.1.1	Experimental setup . . . . .	11
2.1.2	Microscopic processes on crystal surfaces . . . . .	12
2.2	Surface alloying and segregation . . . . .	14
2.3	Theoretical description of heteroepitaxial growth . . . . .	15
2.3.1	Density functional theory . . . . .	16
2.3.2	Molecular Dynamics simulations . . . . .	16
2.3.3	Monte Carlo simulations . . . . .	17
2.3.4	Continuum equations . . . . .	19
2.3.5	Lattice gas vs. off-lattice models . . . . .	20
<b>3</b>	<b>Model and methods</b>	<b>23</b>
3.1	Structure of the fcc lattice . . . . .	23
3.2	The potential energy surface . . . . .	24
3.3	Interaction potential . . . . .	25
3.4	Calculation of the activation energy . . . . .	26
3.4.1	Search for the saddle point . . . . .	26
3.4.2	Binding energy . . . . .	27
3.5	Monte Carlo simulations . . . . .	28
3.5.1	Rejection-free method . . . . .	28
3.5.2	Algorithm . . . . .	29
3.6	Simplifications . . . . .	30
3.7	Conclusions . . . . .	30
<b>4</b>	<b>Equilibrium simulations</b>	<b>33</b>
4.1	The Model . . . . .	34
4.2	Influence of model parameters . . . . .	37
4.2.1	Misfit and interaction energy . . . . .	37
4.2.2	Interaction potential . . . . .	41
4.2.3	Concentration of components . . . . .	43

---

4.2.4	Temperature . . . . .	46
4.3	Conclusions . . . . .	49
<b>5</b>	<b>Growth simulations</b>	<b>51</b>
5.1	The growth model . . . . .	51
5.1.1	Off-lattice Kinetic Monte Carlo simulations . . . . .	52
5.1.2	Ball and spring model . . . . .	52
5.2	Energy barriers . . . . .	53
5.2.1	Diffusion on plane surfaces . . . . .	53
5.2.2	Barriers at step edges . . . . .	56
5.3	Influence of misfit and interaction energy . . . . .	57
5.3.1	Binary systems . . . . .	58
5.3.2	Ternary systems . . . . .	60
5.4	Comparison with equilibrium simulations . . . . .	65
5.5	Conclusions . . . . .	66
<b>6</b>	<b>Conclusions and outlook</b>	<b>69</b>
<b>A</b>	<b>Lennard-Jones potential</b>	<b>71</b>
<b>B</b>	<b>Equilibrium distances</b>	<b>73</b>
<b>C</b>	<b>Evolution into equilibrium</b>	<b>75</b>
	<b>Bibliography</b>	<b>78</b>



# Chapter 1

## Introduction

In recent decades, surface and interface physics has become an increasingly important subdiscipline within the physics of condensed matter. Even though surface phenomena have been studied and some basic theoretical concepts have been developed already afore, the inception of modern surface science dates back to the early 1960s [1, 2], since which essential knowledge in the field of surface science has been found and many experimental techniques have been developed. There are several driving forces for the development of surface physics, among them, e.g., semiconductor technology, the development of new materials and epitaxy.

Within the last decades, many possibilities in the experimental as well as in the theoretical domain have arisen. Many experimental techniques enable the production of very pure materials and the studies of them on a microscopic scale. From the theoretical point of view the progress is related to the wide ability of high-capacity computers and the immense increase of their power. Today, theoretical methods in combination with the use of computers are very important tools in support of design and development of new technical applications. But a microscopic understanding of the growth processes requires the investigation of the surface processes at an atomic level. In this context computer experiments in form of simulations play a very important role.

In this work we treat the simulation of multi-component alloys on surfaces growing by molecular beam epitaxy, which is a very important method to produce high quality crystals with nanostructures on them. Even the use of materials with different lattice constants could lead to interesting phenomena. We focus on the question about the influence of some parameters like, e.g., the lattice mismatch on the pattern formation, what can be conducive to a better understanding of the microscopic processes occurring during the epitaxial production of crystals.

Chapter 2 gives a brief overview of the technical aspects of the molecular beam epitaxy, the single processes which are occurring during this experimental technique, and some concepts of theoretical description. In chapter 3, the model used in the simulations and the basic methods are presented. Chapter 4 is devoted to the pattern formation in equilibrium simulations and chapter 5 deals with the

results of growth simulations and draw a comparison to the findings in the chapter before. Finally, chapter 6 gives a résumé of this work and an outlook on further possible investigations in this field.

# Chapter 2

## Theoretical background

In this chapter the principles of molecular beam epitaxy, which forms the experimental basis of this work, are shortly described. After this some theoretical methods for modeling this technique are presented.

### 2.1 Molecular beam epitaxy

Molecular beam epitaxy (MBE) is an experimental technique to produce very pure crystals [3], for example by deposition of a crystalline phase on a substrate crystal. There, the growing layer is strongly influenced by the physical properties of the substrate [4]. In principle, one distinguishes between homoepitaxy and heteroepitaxy. In the case of homoepitaxy the grown layers consist of the same material as the substrate, in contrast to heteroepitaxy, where different materials are used which may have different properties like, e.g., the lattice constants.

MBE is used for the production of high-quality crystals and the engineering of well controlled alloy compositions. Implementations of this technique are important in many technical applications today, e.g. components in nanoelectronics, computer technology, or telecommunication domain.

#### 2.1.1 Experimental setup

Fig. 2.1 shows schematically the setup of an MBE chamber [5]. In the chamber, an ultrahigh vacuum (UHV) is maintained in order to avoid unintended impurities and for producing crystals as pure as possible. The solid source materials are placed in effusion cells and the substrate is positioned on a heatable base, which can be rotated to improve the growth homogeneity.

One very important aspect of MBE is the slow deposition rate ( $10^{-3}$  to 1 atom layers per second), which allows the films to grow epitaxially. However, the slow deposition rates require excellent vacuum conditions in order to achieve the same purity levels as other deposition techniques. The materials, which are to

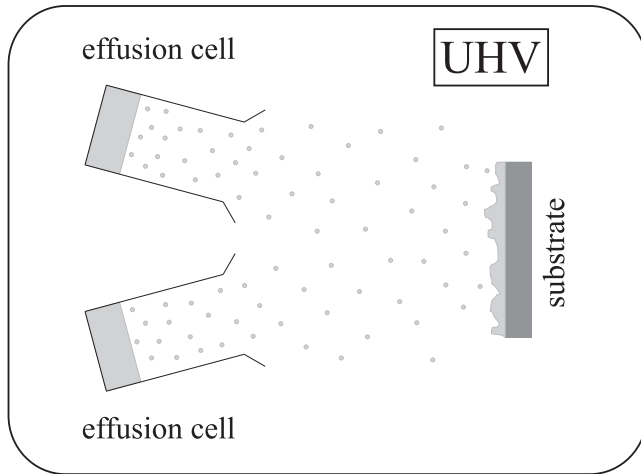


Figure 2.1: Setup of an MBE chamber with effusion cells and substrate in an ultrahigh vacuum environment.

be deposited on the substrate, are heated in the effusion cells until they begin to evaporate. The evaporated elements then condense on the wafer, where they may react with each other and build an adsorption layer. The term “beam” simply means that evaporated atoms do not interact with each other or any other chamber gases until they reach the wafer, due to the long mean free paths of the beams. The particle flux can be controlled by regulating the temperature of the heating. The flux and the temperature of the substrate have an essential influence on the growth of the crystal. Thereby, the growth can be regulated very exactly, so single atom layers (so-called monolayers) can be deposited on the substrate. During this process the growth can be well monitored in situ on an atomic scale by reflection high-energy electron diffraction (RHEED), for instance.

### 2.1.2 Microscopic processes on crystal surfaces

When the evaporated adsorbate materials reach the substrate several microscopic processes on the surface are possible [6, 7] as shown in Fig. 2.2. First, there is the process of *deposition*, which results in the adsorption of the atom. After this, the particle has the possibility to *desorb* and leave the crystal again or to *diffuse* on the surface until a binding site is reached, which is energetic favorable. In the following we give a conceptional description of the processes which play an essential role in epitaxial growth.

#### Deposition

The molecular beam arrives with a certain flux  $F$  (usually measured in monolayers per second) the substrate and the particles of this beam can incorporate or perform the so-called downhill funneling [8], whereas they slide down a slope until they reach a position with a maximum number of neighbor particles.

After the deposition an adsorbed atom (adatom) can move on the surface,

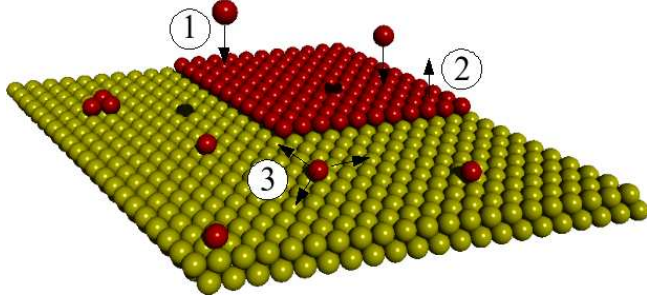


Figure 2.2: Schematic illustration of the relevant processes during MBE growth: Deposition(1), desorption(2), and diffusion(3).

because the arriving particle usually has a considerable kinetic energy due to the high temperature in the effusion cell.

### Desorption

After a particle is deposited and bound to the crystal it might desorb again. That means that the adatom leaves its binding site and evaporates into the MBE chamber. This process depends on the binding energy  $E_b$  and occurs according to the desorption rate  $R_{des}$  defined by the Arrhenius law:

$$R_{des} = \nu_0 e^{-\frac{E_b}{kT}} \quad (2.1)$$

where  $k$  is the Boltzmann's constant,  $T$  the temperature, and  $\nu_0$  the attempt frequency, which is on the order of the Debye frequency of the crystal ( $\nu \approx 10^{12} \text{ s}^{-1}$ ).

In comparison to the rates of deposition and diffusion the desorption rate is small because of the high characteristic binding energies of about  $2.5 \text{ eV}$ . For this reason, desorption can be neglected for many materials, provided the substrate temperature is not too high.

### Diffusion

Because of thermal fluctuations every adatom which is not completely enclosed can diffuse on the surface, searching for energetically favorable positions. The particle performs “jumps” from one binding site on the lattice to a neighboring binding site. Every binding site corresponds to a minimum in the potential energy surface of the crystal, and at this position the adatom is strongly bound to the crystal. The surface diffusion is an activated process with a rate according to the Arrhenius law:

$$R_{dif} = \nu_0 e^{-\frac{E_a}{kT}}. \quad (2.2)$$

The activation energy  $E_a$  is the barrier which has to be overcome for a step. This energy depends on the energy of the binding site  $E_b$  at the beginning and the energy at the transition state  $E_t$  between the two sites:

$$E_a = E_t - E_b. \quad (2.3)$$

The transition state corresponds to a saddle point of the potential energy of the system. Depending on the configuration the particles might diffuse on the plane surface or along step edges of islands.

In addition to the hopping diffusion there is a further possibility for movement on the surface. A mobile particle can exchange its position with a particle which is integrated in the lattice [9]. Then the, so far, immobile atom takes the role of the adatom and diffuses on the surface. This process is called exchange diffusion and its frequency depends on the local crystal configuration and the used materials [10–12]. In some materials this mechanism plays a big role at the movement along step edges, for example.

But an adatom which is moving along a step edge can also break away from this edge. The probability of this mechanism depends on the strength of the bonds between the particle and the edge.

## 2.2 Surface alloying and segregation

The formation of surface alloys is of particular interest. Experimental studies show that many materials which are immiscible in the bulk form stable alloy layers if they are deposited as thin films on certain substrate materials. This phenomenon can be observed in a variety of systems. Here, a very important aspect is the influence of the different lattice constants of the involved materials on the detailed structure. In order to minimize the energy, the lattice mismatch may lead to formation of certain structures like, e.g., stripes on the nanometer scale. The resulting formation can be explained by the interplay of two mechanisms: strain relaxation and kinetic segregation [13–15].

The first one refers to achieving a low effective adsorbate misfit and hence an energetically favorable state by an alternating arrangement of particles with negative and positive misfit with respect to the substrate, see Fig. 2.3. This configuration of the different adsorbate materials yields a state with less strain and lowers the energy.

The second mechanism refers to the separation of the elements with a boundary as short as possible, if the inter-species binding is weaker than that of same species, see Fig. 2.4. The different binding energies can result in a strong kinetic

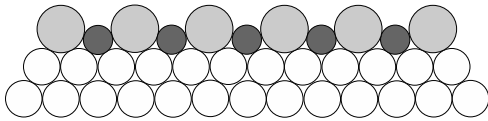


Figure 2.3: Side view of a ternary system with a substrate (white) and two adsorbates (in dark and light gray). Strain relaxation provides an energetically favorable state.

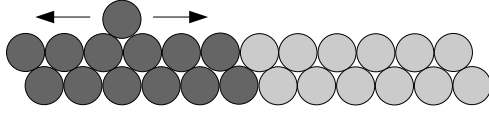


Figure 2.4: Top view of an island existing of two adsorbates with a weak interaction between particles of different materials. Due to the interaction energies a separation is preferred.

effect for diffusion along existing edges [14], which leads to domains containing the same species because of an extra barrier for a particle trying to cross the interface at the edge. Due to the different interaction energies islands with separated areas of each material are energetically favorable. Thus, the different binding energies would prefer a complete segregation of the different components, but in fact the moves of the particles in non-equilibrium growth rather result in smaller structures. If the adsorbate materials are deposited as thin films on the substrate the adatoms move on the surface and try to segregate due to the interaction energies. Clearly, in this context the deposition rate plays an important role and influences essentially the emerging structures.

The interplay of both effects leads to interesting alloy structures like, e.g., stripes or islands. Examples of surface alloyings are systems like CoAg/Ru(0001) [13, 16, 17], AgCu/Ru(0001) [18], PdAu/Ru(0001) [19], CoCu/Ru(0001) [20], CoAg/Mo(110) and FeAg/Mo(110) [15].

## 2.3 Theoretical description of heteroepitaxial growth

In addition to the practical application of the MBE, theoretical investigations of epitaxial growth are very interesting and necessary for the comprehension of the physical processes. In particular studying the influence of specific parameters is important for a detailed understanding of the functioning of epitaxial growth. By dint of theoretical research, particular mechanisms and their influence on the emerging structures can be studied. The findings of these studies can help to enhance experimental techniques and realize new applications in many different domains.

Since MBE is far away from thermal equilibrium, most general theoretical concepts are not suitable for description in this case and new methods of theoretical description are in demand [6, 7, 21–24]. In this work we use Monte Carlo simulations for investigating heteroepitaxial growth [24]. In the following sections, this method and other important approaches providing good descriptions are briefly presented.

### 2.3.1 Density functional theory

The macroscopic growth is based on microscopic processes such as deposition, desorption or diffusion of particles. These processes are mainly affected by changing or breaking chemical bonds. Ultimately, it is necessary to take quantum mechanics into account.

In this context, the density functional theory (DFT) turned out to be a very useful tool to describe growth mechanisms. Originally, DFT is a method which determines the quantum mechanical ground state of a many-particle system from the density of electrons. To this end it is not necessary to solve the complete Schroedinger equation of the system. Instead, the interaction of the particles is taken into account in the form of an exchange potential [25–28]. The basic principle of DFT is the Hohenberg-Kohn theorem, which states that the ground state properties of a system of  $N$  electrons can be represented in terms of only the ground state density. All properties of the ground state can be calculated from the position-dependent electron density  $n(r)$ . Hence, the problem of solving the many electron Schroedinger equation is replaced by finding the appropriate exchange potential and solving the single particle equations, the Kohn-Sham equations [25, 28]. In these equations the so-called local exchange-correlation potential regards the many-particle system. Due to the fact that the exchange-correlation potential in the most cases cannot be determined exactly, approximations are required [29].

Growth mechanisms are essentially conditioned by activated processes with rates depending on energy barriers and attempt frequencies, as described in Sec. 2.1.2. The frequencies may be obtained by using the transition state theory [22]. The DFT method allows for the calculation of energies as well as the exact determination of the positions of the particles on the surface. The resulting knowledge of the barriers and surface configurations enables the description of surfaces or their evolution under different conditions. So, all the relevant information required for describing growth processes can be calculated within the DFT formalism, in principle.

A big problem of the DFT is the large computational effort. This fact limits the method to relatively small systems. However, DFT is a very important tool for the calculation of basic properties of molecules and solid state bodies, like binding lengths, energies, oscillation spectra or magnetic properties, see e.g. [30–34]. Many of these results can be used for further processing in other methods.

### 2.3.2 Molecular Dynamics simulations

In Molecular Dynamics (MD) simulations, used at the first time by Alder and Wainwright in the 1950s [35, 36], the evolution of a system of  $N$  interacting particles is calculated by numerical integration of the classical equations of motion to trace the positions and velocities of the particles [21, 37, 38]. The system can be completely described because all positions and velocities are well known. By



dint of the statistical physics, in principle it is possible to calculate all interesting properties of structure, dynamics and thermodynamics. This method allows simulating systems both at equilibrium and away from equilibrium. Thereby, the used forces are derived from DFT [39] or empirical potentials. Because of computer demands often simple pair potentials are favored in the second case. By use of DFT, correct quantum mechanical forces can be implemented as e.g. in the simulations of Car and Parrinello [39]. There, the ionic forces are determined directly from the electronic structure of the system independently of any empirical parameter.

A big problem of MD are the enormous run times, which restrict the time and length scales that can be simulated. In general the simulated times range from a few  $ps$  to hundreds  $ns$  and the typical system sizes are about  $10^3 - 10^6$  particles [38]. At massively parallel clusters it is possible to simulate systems with up to  $5 \times 10^9$  particles or up to times of  $1\mu s$  for 3000 molecules, but the run times are very long [40]. Indeed, simulations of crystal growth in general require real time scales of minutes or hours. In order to circumvent this difficulty, very often unrealistically high deposition rates are used in growth simulations.

In spite of these problems MD simulations are often used to simulate growth, see e.g. [41–43]. Other possibilities of application are the estimation of rates for different moves of an adatom or the calculation of energy barriers [44]. Furthermore, MD should be a good technique for simulating processes which cannot be described as thermally activated, such as the deposition process. Finally, the use of MD in combination with other methods in a multiscale approach seems promising.

### 2.3.3 Monte Carlo simulations

In Monte Carlo (MC) simulations the processes are treated as stochastic events. At the beginning of the simulation a catalogue of possible events and their rates is set up. Then, at every simulation step one event is randomly chosen according to its probability, in general given by the Arrhenius law (2.2). This procedure can be realized by, e.g., the Metropolis algorithm [45].

#### Thermodynamic Monte Carlo simulations

MC can be used in equilibrium thermodynamics [21]. There, the system moves from one state  $S_n$  to another  $S_m$  with every simulation step. Such a sequence of configurations forms a Markov chain with a distribution which converges to a stationary distribution  $P(S)$  in thermal equilibrium [46]. Here, the average value of a quantity  $A$  is given by  $\langle A \rangle = \sum_S A(S)P(S)$ . For constructing the Markov chain a matrix of transition probabilities, the Markov matrix  $W(S_n \rightarrow S_m)$ , between two states is needed. These probabilities do not need relate to dynamical transition probabilities, as long as the correct stationary density is achieved. The

master equation describes the time dependence of  $P(S)$  [47, 48]:

$$\frac{\partial P(S_n, t)}{\partial t} = \sum_{m \neq n} (W(S_m \rightarrow S_n)P(S_m, t) - W(S_n \rightarrow S_m)P(S_n, t)), \quad (2.4)$$

where the total probability is conserved ( $\sum_n P(S_n, t) = 1$ ). This equation describes a main property of Markov processes: the knowledge of the state at time  $t$  completely determines the future evolution. In equilibrium  $P(S_n)$  is constant in time,  $\partial P(S_n, t)/\partial t = 0$ , and the terms on the right-hand side of the equation must be equal. This demand is satisfied if the Markov chain fulfills detailed balance:

$$W(S_n \rightarrow S_m)P(S_n) = W(S_m \rightarrow S_n)P(S_m), \quad (2.5)$$

implying that the total rate of the transitions  $S_n \rightarrow S_m$  is equal to the rate of  $S_m \rightarrow S_n$ . This is a sufficient, but not necessary condition for the convergence of the Markov chain [21, 46]. Because the equilibrium distribution should be a Boltzmann distribution, the values of  $P(S_i)$  are chosen as Boltzmann probabilities  $P(S_i) = e^{-E_i/kT}/Z$  with the partition function  $Z$ .

In MBE models, the implemented deposition and desorption processes often violate detailed balance since deposition is not an activated process and desorption is an irreversible process because of the perfect UHV in an ideal MBE chamber, where desorbed particles are removed immediately. Frequently attachment processes are also considered to be irreversible and, hence, violate detailed balance.

### Kinetic Monte Carlo simulations

In contrast to simulations in thermodynamical equilibrium in the study of kinetic processes the implemented events and the transition probabilities correspond to real physical events and probabilities, respectively. In Kinetic Monte Carlo (KMC) methods real processes like e.g. diffusion are simulated [21, 23, 24]. Similar to the case of thermodynamical MC a Markov chain is generated by random choice of events, but in KMC this chain represents a physically possible set of events with probabilities proportional to their physical rates.

As discussed in Sec. 2.1.2 every event on the surface occurs according to a rate given by the Arrhenius law,

$$R = \nu_0 e^{-\frac{E_a}{kT}}, \quad (2.6)$$

and the waiting time of an event is accordingly given by

$$\tau = \tau_0 e^{\frac{E_a}{kT}}, \quad (2.7)$$

where the activation energy  $E_a$  is the barrier which has to be overcome by thermal activation. At the process of diffusion a particle jumps from one binding site to a

neighboring one and the activation energy results from the energy of the binding state and the energy of the transition state:  $E_a = E_t - E_b$ . The use of the Arrhenius law is justified in the transition state theory based on the assumption of thermal equilibrium situation at the occupation of binding and transition state as discussed e.g. in [22].

By using the same attempt frequency  $\nu_0$  in Eq. (2.6) for all diffusion processes the condition of detailed balance (2.5) with Boltzmann probabilities is fulfilled:

$$\frac{R_{n \rightarrow m}}{R_{m \rightarrow n}} = e^{-\frac{E_{b,m} - E_{b,n}}{kT}}, \quad (2.8)$$

with the rate  $R_{n \rightarrow m}$  of a jump from site  $n$  to the neighboring site  $m$  and the rate  $R_{m \rightarrow n}$  of the backward jump.

KMC simulations also can be combined with continuum methods. An example of such a hybrid method is the method introduced by Russo, Sander, and Smereka [49]. In this so-called quasicontinuum Monte Carlo method the motion of adatoms is treated in continuum theory, but at attachment process the particle is represented individually. The implementation of this technique could be interesting if there is a large separation of time scales between the diffusion of adatoms and fluctuations of island boundaries. A similar hybrid method is presented by Schulze in [50].

The big advantage of MC is the realizable time scales of simulations, which can range up to a few 1000s, although for larger systems the computer time effort increases to high values. The MC method can be used, e.g., for investigating the evolution of morphology, kinetics of growth or scaling exponents.

### 2.3.4 Continuum equations

The simplest growth model is the model of random deposition (RD). There, a particle falls vertically from a randomly chosen site over the surface until it reaches the surface, whereupon it is deposited and sticks to this position [7]. A little bit more realistic is the random deposition model with surface relaxation. In this model, the particle can diffuse after deposition until it finds the position with the lowest height, but the diffusion is stopped if a maximum number of moves is reached. Here, the surface becomes substantially smoother than in the simpler RD model.

Simple growth processes like the above can be described by continuum equations [7] of the form

$$\frac{\partial h(r, t)}{\partial t} = f(r, t) \quad (2.9)$$

with the surface height  $h(r, t)$  and a function  $f(r, t)$  describing the number of particles per unit which are incorporated at position  $r$  and time  $t$  on the surface. Considering symmetry arguments [7] this function can be divided in a sum of

two terms: a combination of powers of  $\nabla^n h$  and a noise term  $\eta(r, t)$  reflecting the random fluctuations in the deposition process. Then, in the simplest case the growth in the model with the surface relaxation can be described by the Edwards-Wilkinson (EW) equation [7, 51]:

$$\frac{\partial h(r, t)}{\partial t} = \nu \nabla^2 h(r, t) + \eta(r, t). \quad (2.10)$$

The first term of the right-hand side describes the smoothing effect of the interface relaxation by a surface tension  $\nu$  and  $\eta(r, t)$  is the noise term, which is a Gaussian distribution.

If one adds a nonlinear term of form  $(\nabla h)^2$  to the EW equation one attains to the Kardar-Parisi-Zhang (KPZ) equation [7, 52, 53]:

$$\frac{\partial h(r, t)}{\partial t} = \nu \nabla^2 h(r, t) + \frac{\lambda}{2} (\nabla h(r, t))^2 + \eta(r, t). \quad (2.11)$$

The second term is the lowest-order nonlinear term that can appear in the interface growth equation and reflects the presence of lateral growth. Only by implementation of this nonlinear term some properties of growing interfaces are explainable. In general higher-order terms are not relevant and can be neglected for describing growth.

### 2.3.5 Lattice gas vs. off-lattice models

Two major classes of models for the simulation of growth can be considered: on the one hand lattice gas models with discrete binding sites [23] and on the other hand more realistic off-lattice models using continuous coordinates [24, 54].

In the case of lattice gas models, see e.g. [55], the system provides discrete sites and each particle can only be located on such a predefined site. Thus, every lattice site is either empty or occupied. In the diffusion process a particle jumps from one discrete binding site to another, i.e. the first site becomes empty and the second becomes occupied. This method is ideal for use in simulations in which all the particles have the same lattice constant, e.g. the simulation of homoepitaxy. In general lattice gas models have a good computing performance because it is not necessary to calculate the exact positions of the particles, but it is only necessary to manage a set of integer variables representing the occupation states of the sites. However, this method rules out some important effects like the formation of dislocations.

An alternative method is the use of off-lattice, continuous space models, in which the particles can be located in continuous positions independent of any lattice. Obviously, this is of particular importance in the simulation of heteroepitaxial systems where the lattice constants of the deposited adsorbates may differ from that of the substrate. Some interesting phenomena like the formation of

dislocations in crystal can only be simulated if the particles may move independent from predefined sites, see e.g. [56,57]. But here it is not possible to describe the system by use of a simple set of integer variables and the consequence of this modeling are significantly larger simulation times.

In this work we focus on the simulation of heteroepitaxial systems. Hence, it is necessary to use an off-lattice framework for reproducing very interesting effects resulting from different lattice constants of the materials. Especially the investigation of alloy structures caused by strain effects requires the use of off-lattice models.



# Chapter 3

## Model and methods

Many crystals, which are interesting for technical applications, build a *face centered cubic* (fcc) lattice, for example metals like Cu, Pt, Au, Al or Ni. Furthermore, alloys of many metals are arranged in an fcc lattice. In this work we simulate epitaxial growth of fcc crystals in the [111] direction.

In this chapter we explain the structure of the fcc lattice and the corresponding construction of fcc crystals in computer simulations. Thereafter, the used potential, the model, and methods are presented in detail.

### 3.1 Structure of the fcc lattice

In the fcc lattice, which is a Bravais lattice, eight atoms are collocated so that they form the corners of a cube, and six further atoms are located in the center of every face of this cube [58,59]. This configuration has the highest average density of about 0.74, corresponding to a closed packing of spheres. Fig. 3.1 (a) shows the according unit cell, which has four atoms in it:  $1/8$  atom in every corner and  $1/2$  atom on each face resulting in  $8 \times 1/8 + 6 \times 1/2 = 4$  atoms. In this crystal structure the coordination number is twelve.

Each of the planes drawn in Fig. 3.1 (a) represents a layer of the crystal in the [111] direction. In every layer there is a triangular lattice, but the lattices of two successive layers are moved against each other.

Fig. 3.1 (b) shows a look in the [111] direction with a first layer A of gray-colored particles and a few particles of a second layer B upside layer A, colored in black. In a third layer, there are two possibilities to arrange the particles [60]. If atoms are placed directly above the atoms of the first layer (e.g. the gray-colored particle on the left-hand side) and the atoms of the fourth layer above the atoms of the second layer etc., one get an ABABAB... stacking which accords to *hexagonal close-packed* (hcp) structure. Another possibility is to put the atoms of the third layer C above the spaces of the first layer (e.g. the white-colored particle on the right-hand side) and subsequently the atoms of the fourth layer directly above the

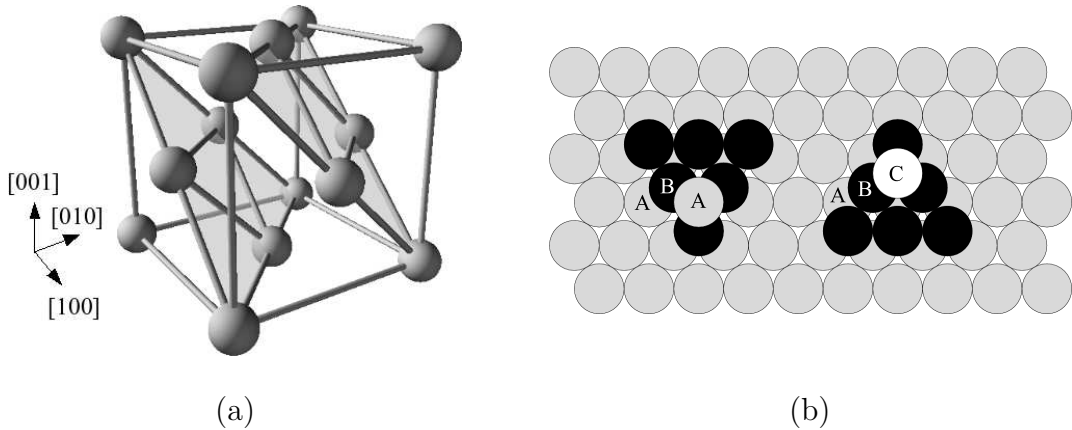


Figure 3.1: (a) Left-hand side: illustration of fcc lattice structure. The drawn planes represent the crystal layers in the  $[111]$  direction pointing perpendicular to the planes. (b) Right-hand side: hcp lattice (left) and fcc lattice (right).

atoms of the first layer etc. Thus, one gets an ABCABC... stacking representing the fcc lattice.

## 3.2 The potential energy surface

Our method is based on the work by Schindler and Wolf [61] and the main idea is to calculate the energy barriers for all occurring events and to use the according rates in a rejection-free simulation. The energy surface resulting from the existing structure and the potential has the essential influence on all processes upon the crystal surface. As already described in Sec. 2 the activation energy in a diffusion process is given by the difference of the energies at the transition state and the binding site. The binding site corresponds to a minimum in the *potential energy surface* (PES) [62] and the transition state is represented by a first order saddle point in the energy landscape [29]. Therefore the knowledge of the geometry and the form of the PES is very important for the calculation of the activation energy and the rates for the diffusion events in the simulation.

Computing the PES requires the reconstruction of the crystal at first. For that purpose a few layers of an fcc crystal are built up as depicted in Fig. 3.1. After that a test particle is moved in small steps across the constructed surface and after each step the total potential energy of the system is minimized by variation of all particle coordinates in the crystal plus the test particle's  $z$  coordinate perpendicular to the surface. The potential energy and the plane-parallel coordinates of the test particle yield the PES. Fig. 3.2 shows an example of such an PES for a plane surface. The minima in that landscape represent the possible stable binding sites of the test particle and the intermediate saddle points the metastable transition sites. The locations of the maxima indicate the positions of



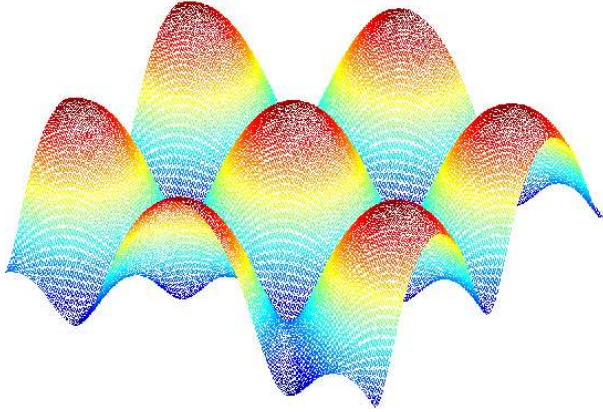


Figure 3.2: Potential energy surface calculated for a test particle on a plain crystal surface. The crystal consists of an fcc lattice.

the particles incorporated in the upper substrate layer. Positioning directly onto these particles is most unfavorable for the test particle. Therefore the adatom would have its highest potential energy there represented by a maximum in the PES.

In every diffusion step a particle jumps from one binding site to another whereas a barrier according to the activation energy has to be overcome. Therefore it is required to compute the location of the corresponding saddle point and the energy at this position. Some geometrical considerations can simplify the calculations and accelerate the simulation.

### 3.3 Interaction potential

The PES and consequently all relevant sites are the result of the potential used in the simulations. To keep the computational effort within a feasible limit we use simple pair potentials in all our simulations in this work. In the majority of cases we choose the Lennard-Jones 12,6 potential [58]:

$$U_{ij} = 4 E_{ij} \left[ \left( \frac{\sigma_{ij}}{r_{ij}} \right)^{12} - \left( \frac{\sigma_{ij}}{r_{ij}} \right)^6 \right]. \quad (3.1)$$

Here,  $E_{ij}$  is the potential depth and  $r_{ij}$  the distance between the two interacting particles  $i$  and  $j$ . The potential is zero at  $r_{ij} = \sigma_{ij}$ . Thus, the parameter  $\sigma_{ij}$  controls the equilibrium distance of two isolated particles  $r_{ij}^0 = 2^{1/6} \sigma_{ij}$  and depends on the interacting materials. Hence, the lattice constant in an undisturbed monoatomic system of element  $i$  would be directly proportional to  $\sigma_{ii}$ . For definition of the generalized Lennard-Jones n,m potential see appendix A.

In our simulations the potential is cut off at a distance  $r_{cut} = 3 r_{ij}^0$ , which is justified due to the fact that the potential has a steep form and converges fast to  $U_{ij} = 0$  for increasing  $r_{ij}$ . This approximation allows a cheaper computation of the potential, especially if a system with many particles should be simulated.

## 3.4 Calculation of the activation energy

The diffusion plays an essential role in epitaxial growth. Therefore the calculation of diffusion rates is one of the main requests during the simulation. In the process of surface diffusion the adatom moves from one binding site on the lattice to another and according to the Arrhenius law (cf. Sec. 2.1.2) the activation energy  $E_a = E_t - E_b$  has to be overcome for each diffusion step. On that account the goal is to compute the energies at the transition site  $E_t$  and at the binding site  $E_b$ .

As described in Sec. 3.2 the transition site corresponds to a saddle point in the potential energy surface (PES). For this reason the exact location of the saddle point between the two binding sites (and the energy at this position) has to be calculated. In addition the minimum in the PES representing the binding site has to be determined.

### 3.4.1 Search for the saddle point

For finding saddle points there are no general methods which are guaranteed to work. However, the saddle search algorithm of the so-called *activation-relaxation technique* (ART) turned out to be a good method in the case of our energy landscapes. In this technique the saddle point is found by using an iterative algorithm [63–65], the steps in detail are:

1. The adatom is slightly moved from its actual binding site in the estimated direction of the next minimum.
2. The particle is moved a small step in direction of the redefined force

$$\vec{G} = \vec{F} - (1 + \alpha) (\vec{F} \cdot \vec{e}) \vec{e} \quad (3.2)$$

with  $\alpha > 0$ , the acting force  $\vec{F}$  and the unit vector  $\vec{e}$  pointing from the last minimum to the current position of the particle. The force  $\vec{G}$  points to the saddle point, so that the particle is pushed into the wanted direction.

3. The last step is repeated until the saddle point is reached and  $\vec{F} = \vec{G} = 0$ .

The force  $\vec{F}$  is resulting from the potential and is zero at minima, maxima and saddle points in the energy landscape. The number  $\alpha$  controls the increment in each iteration step, values between  $\alpha = 1.0$  and  $\alpha = 2.0$  lead to good results. By contrast, too small values result in too many iteration steps during saddle point search and too high values in missing the saddle point.

In principle, it would be necessary to relax the whole system in every step of the saddle point search. That means that in every step the positions of all particles in the crystal should be changed so that the total energy reaches a local

minimum and the crystal is relaxed. The *frozen crystal* approximation, in which only the adatom's position is varied and all other particles are fixed, leads mainly to a small shift of all barriers to higher values [66]. However, this simplification yields a big speed-up of simulation time. For this reason we use the frozen crystal approximation during searching for the saddle point.

A computationally less demanding method of determining the transition energy is to calculate the energy at the saddle point by considering the number of particles in the neighborhood. This method has its origin in the *ball and spring model*, where the hopping activation energy depends on the bonding environment and the elastic energy associated with strain [67–71]. In this technique the activation energy is calculated from bond and strain energy  $E_a = E_{bond} - E_{strain}$ . Here, the strain energy  $E_{strain}$  is the elastic energy difference of the system when the site is unoccupied and when the site is occupied. The elastic energy is given by harmonic interactions between an atom and its neighbors, using spring constants. However, the bond energy  $E_{bond}$  depends on the number of occupied nearest and next-nearest neighbors. This model describes many phenomena, but it can not be used for simulation of misfit dislocations.

However, the number of occupied nearest and next-nearest neighbors can be used to determine the energy at the saddle point  $E_t$ . With that information the activation energy  $E_a = E_t - E_b$  could be calculated, if the binding energy is known. The advantage of this method (with the exact binding energy) is that the determined barrier is more realistic than in the case of pure ball and spring, but fast in comparison to calculating the exact saddle point.

### 3.4.2 Binding energy

In addition to the energy at the saddle point the energy at the binding site has to be calculated. However, the binding energy is computationally much easier to determine than the transition energy at the saddle point. In most crystal configurations it is effortless to guess the position of the binding site by geometrical considerations. After the adatom is placed to the approximate position the particle reaches the exact binding site with the binding energy  $E_b$  by relaxation of the system.

The diffusion process of an adatom influences the other particles of the system around its position. Due to the new adatom the particles feel a different potential than before and as a result their positions change. In consideration of this the environment of the adatom has to be relaxed after every diffusion or deposition event. This is done by minimizing the total potential energy of the system,

$$E_{tot} = \sum_{i<j} U_{ij}, \quad (3.3)$$

by using a standard conjugate gradient method as described e.g. in [72]. To save computer time only a local relaxation is performed. Thereby, solely the

particles within a sphere of radius  $r_{cut}$  around the adatom are treated and their positions are changed according to the potential energies. Taking into account that the change of these positions influence the potential energies of particles within a sphere of radius  $2r_{cut}$ , the diffusion barriers within this radius have to be recalculated and the according rates have to be updated (see next section).

To avoid strain generated by using only the local relaxation, a global relaxation after a certain number of steps (1000 in the most cases) has to be performed. This ensures a simulation without artificial strain caused by local relaxation, but the computational effort is kept within a manageable range.

## 3.5 Monte Carlo simulations

There are different possibilities to realize the stochastic Monte Carlo kinetics. The implementation of simple techniques, which simulate the Markov chain defined in Sec. 2.3.3 directly, leads to a slowing down of the simulation. This originates from the fact that in many simulation steps the state of the system remains the same.

In methods like the Metropolis algorithm [45] in every step an event is selected and its rate is calculated, but the event is accepted only with a certain probability according to its rate. This procedure leads to many events which are rejected and do not change the system at all. Thus, especially at low temperature the probability of a not-modifying step is high and many events are calculated, but not performed.

### 3.5.1 Rejection-free method

In order to avoid time-consuming computations of events which will be rejected, continuous time algorithms are used, examples are presented in [46, 73, 74]. In consideration of this aim in every simulation step an event is selected according to its rate and performed. In this rejection-free method only steps modifying the system are taken into account. The required bookkeeping slows down the simulation, but the speed-up by avoiding rejected events outweighs and leads to a larger saving in time, especially at low temperatures.

In our rejection-free algorithm a modifying event  $i$  is selected and performed according to its probability

$$p_i = \frac{R_i}{R_d + \sum_j R_j}. \quad (3.4)$$

Here,  $R_i$  is the rate of the event  $i$  and  $R_d$  the deposition rate. The physical time  $\tau$  this event would take is exponentially distributed with a probability density

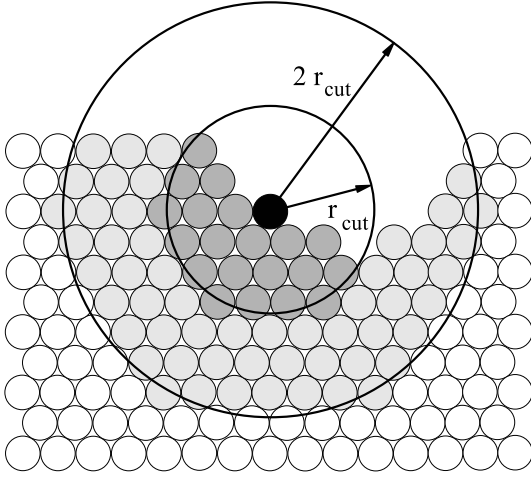


Figure 3.3: Environment of a moved particle in 2 dimensions. The particles within a radius of  $r_{cut}$  (colored in dark gray) have to be relaxed and all rates of the particles within the outer circle (in light and dark gray) have to be recalculated.

$P(\tau) = R e^{-R\tau}$ , where  $R$  is the sum of the rates of all events [75], and is given by

$$\tau = - \frac{\ln \rho}{R_d + \sum_j R_j} \quad (3.5)$$

with an uniformly distributed random number  $\rho \in ]0, 1]$ .

### 3.5.2 Algorithm

At the beginning of the simulation a catalogue with the rates of all modifying events, which could potentially occur, is set up. For that purpose the rates of all possible events have to be calculated.

After computation of the binding energy  $E_{b,i}$ , the transition energy  $E_{t,i}$ , and the resulting activation energy  $E_{a,i}$  the rate of each possible diffusion or desorption event  $i$  could be calculated according to the Arrhenius law  $R_i = \nu_0 e^{-\frac{E_{a,i}}{kT}}$ . Moreover, the rate of a deposition event  $R_d$  results from the particle flux.

Following the work of Ahr [76] the rates are saved in a complete binary tree, from which particular events will be selected during the simulation. The rejection-free method is realized as follows:

1. An event  $i$  is drawn according to its probability  $p_i = R_i/R$  and performed.
2. The crystal is locally relaxed around the location of the event and the rates of all events affected by the local relaxation are recalculated. The search tree is updated.
3. The time is increased by the time interval  $\tau = -\ln \rho/R$ , Eq. (3.5).
4. If the condition for a global relaxation is met the complete system is relaxed and all diffusion rates are recalculated. The search tree is updated.

5. The steps 1 to 4 are repeated until a terminating condition is fulfilled.

Here, the sum of all rates is given by  $R = R_d + \sum_j R_j$ . In step 2 it is obvious that the interaction energies of many particles may be changed by the local relaxation and all affected rates have to be recalculated. Assuming that the particles around a distance of  $r_{cut}$  have been relaxed the rates of all particles within a radius of  $2r_{cut}$  have to be updated. Fig. 3.3 shows an illustration for the 2-dimensional case.

### 3.6 Simplifications

To keep the computational effort within a manageable limit some simplifications are required. As aforementioned only simple pair potentials are used to represent the interactions between the particles and, due to the fact that the Lennard-Jones potential is very weak for large distances, the interaction is cut off at a certain distance  $r_{cut}$ .

But further simplifications can be implemented in order to reduce the simulation time. The frequency of some processes is very small in comparison to that of others, so that these processes may be excluded explicitly. For instance, the desorption process is neglected due to the fact that the desorption rate is small compared to diffusion or deposition for many materials. Thus for large enough flux the time required for adding a monolayer may be much smaller than the waiting time for a desorption event.

In this work we focus on the simulation of growth in the first adsorbate layer. Particles which are deposited upon an existing island of the first monolayer diffuse on this island until they reach the step edge. The rate of a downward jump decides on which probability the particle jumps down or not. But for a finite energy barrier of this process the particle jumps down after a finite time and arrives at the first monolayer. In addition upward jumps into the second layer may be forbidden because of the very large barrier. Therefore all important activities of the adatoms in our simulations take place in the first monolayer, in which every particle ends up at any time at all, and the movement of second layer particles can be excluded in our simulations.

### 3.7 Conclusions

In the beginning of this chapter we have described the fcc crystal structure. If one focus on the growth in the [111] direction a triangular lattice is observed in each layer. Here, the adatoms may occupy fcc or hcp sites which result from an ABCABC... or ABABAB... stacking of the layers being located on top of each other.

The potential energy surface resulting from the particle interactions controls all growth mechanisms. Minima in the energy landscape represent binding sites on the crystal surface and the saddle points correspond to the transition sites during diffusion processes. The particle interactions are realized by using the Lennard-Jones potential which is cut off at a distance  $r_{cut}$  due to the convergence of the potential to zero for large ranges.

For the calculation of the rates it is necessary to compute the activation energies of the particular events which may occur. For this purpose the saddle point search of the activation relaxation technique is implemented in our simulations. Here, the saddle point is determined by moving a test particle step by step in direction of a redefined force. Then the energy at the transition site and the binding site can be calculated and yield the corresponding activation energy. A faster, but less exact method for determining the transition energy is to calculate the energy from the number of occupied nearest and next-nearest neighbors.

Our simulation of epitaxial growth is based on a rejection-free algorithm which allows a computationally more convenient approach than simple straight forward methods. Especially at low temperatures many rejections of randomly selected events would occur and the simulation time would increase.

Some simplifications keep the computational effort of our simulations within a manageable range. For many material systems the process of desorption can be neglected due to its very small rates. Since we focus on growth in one monolayer the movements of second layer particles are also neglected.





# Chapter 4

## Equilibrium simulations

In metal epitaxy, the formation of surface alloys is of particular interest. Often, the involved elements form alloys in thin films on the surface [77]. Here, typical structures are arrays of single dots, so-called droplets, or stripes. In particular multicomponent systems are promising with respect to technical applications. Therefore, in experiments many material systems have been investigated in the last years, examples are CoAg/Ru(0001) [13, 16, 17] or PdAu/Ru(0001) [19].

The emerging structures keep the system in a state with strain as small as possible. In this context surface alloying is a strain reducing mechanism. As described in chapter 2 the interplay between strain relaxation and kinetic segregation results in structures with minimal energy. Lattice mismatches and different chemical and elastic interactions can lead to formation of regular patterns [77], e.g. droplets or stripes studied in [78–82], but further parameters like the concentrations of the different components or the temperature have also an essential influence on the formation of structures.

The alloying can lead to a changing in the morphology of the grown films. An example for such a behavior is CoAg/Ru(0001): if deposited alone onto the substrate, both Co and Ag form compact islands. However, their co-deposition leads to a formation of ramified islands [13] consisting of alternating veins, see Fig. 4.1. As supposed in [13] the different interaction energies yield an extra barrier for a particle trying to cross the interface at the edge of a vein structure. Hence, the particles prefer the observed vein structure and the dendritic island shape. In this context it is of particular interest which microscopic mechanisms are involved in detail. Another important point is the investigation which role the interplay between lattice mismatch and different interactions plays. Just the combination of both effects leads to very interesting alloy structures observed in many experimental studies.

In this chapter we focus on investigations of alloying in equilibrium. To get results in a feasible time a special approach is required. We describe the used simulation model in the next section and present some results afterwards. The influence of different parameters on the emerging structures can be investigated

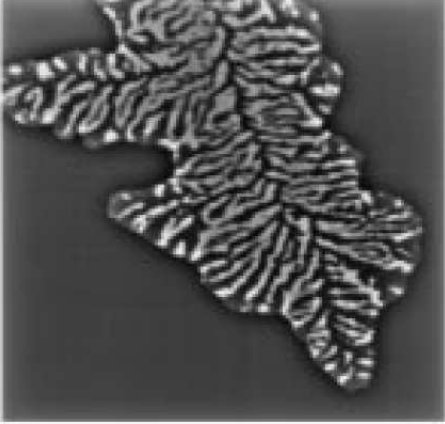


Figure 4.1: 5000 nm x 5000 nm scanning tunneling microscopy image of a dendritic CoAg island on Ru(0001) (taken from Ref. [13]).

excellently with Monte Carlo simulations: many different effects can be switched on and off selectively. Hence, the consequences of single effects on the alloy structures can be analyzed.

## 4.1 The Model

Our aim is to study the formation of alloy structures in 2+1 dimensions in a single atomic layer on the substrate. At first a relaxed substrate crystal has to be reconstructed. Here, we prepare an fcc crystal of seven layers in the [111] direction, which are relaxed and without any strain. The exact composition is described in Sec. 3.1. Here, the distance between two particles is determined to  $r_{SS}^0 = 1.090 \sigma_{SS}$ , for detailed calculation of equilibrium distances in an fcc crystal see appendix B. In the simulations the three bottom layers are kept fix in order to stabilize the crystal structure. All particles in these layers are immobile and, hence, are not relaxed after any step during the simulation.

We model a ternary system of a substrate and two adsorbate materials [83]. In the following, we denote the substrate as  $S$  and the adsorbates as  $A$  and  $B$ .

For calculating the interaction between the particles we use a simple pair potential, namely the Lennard-Jones 12,6 potential:

$$U_{ij} = 4 E_{ij} \left[ \left( \frac{\sigma_{ij}}{r_{ij}} \right)^{12} - \left( \frac{\sigma_{ij}}{r_{ij}} \right)^6 \right], \quad (4.1)$$

where the subscripts  $i, j \in \{A, B, S\}$  specify which elements are involved (see Sec. 3.3). For comparison we use the generalized Lennard-Jones  $n, m$  potential with exponents different from  $n = 12$  and  $m = 6$  (c.f. appendix A) in some cases. In order to speed up the required calculations of potential energies, we cut off the interactions for distances larger than  $r_{cut} = 3 r_{SS}^0$ .

In principle, we do not aim at material specific simulations, our goal is a qualitative understanding of mechanisms that govern two-dimensional alloy for-

mation in a ternary system. Hence, we restrict the choice of parameters  $E_{ij}, \sigma_{ij}$  to simple situations which capture only the most essential features of the pattern formation process. We use the briefer notation  $E_i = E_{ii}$  and  $\sigma_i = \sigma_{ii}$ . Thus, the parameter  $\sigma_S = \sigma_{SS}$  defines the unit of length in the following, i.e.  $\sigma_S = 1$ .

Since the lattice spacing is proportional to  $\sigma$  [58] the relative misfit  $\varepsilon$  results directly from  $\sigma_S$  and  $\sigma_A$ :

$$\varepsilon = \frac{\sigma_A - \sigma_S}{\sigma_S}. \quad (4.2)$$

With respect to the misfit relative to the substrate we study symmetric configurations with  $\sigma_A = 1 - \varepsilon$  and  $\sigma_B = 1 + \varepsilon$  ( $\varepsilon > 0$ ) for the two adsorbates  $A$  and  $B$ . The adsorbate energies  $E_A, E_B$  are chosen equal and their magnitude is fixed relative to  $E_S$ :

$$E_A = E_B = \frac{E_S}{6}. \quad (4.3)$$

Due to this choice the interaction between substrate particles is very strong and the diffusion of substrate particles, as well as interdiffusion of substrate and adsorbate, can be neglected. For this reason no intermixing of substrate and adsorbate materials can occur.

In order to keep the number of free parameters small we follow a standard approach and set for interaction involving different materials in the following way:

$$E_{iS} = \sqrt{E_i E_S} \quad \text{and} \quad \sigma_{ij} = \frac{\sigma_i + \sigma_j}{2}$$

where  $i, j \in \{A, B, S\}$ . (4.4)

The energy  $E_{AB}$  is of special interest and varied separately instead of been calculated by the square root.

In all our simulations we consider hexagonal substrate regions with fixed boundary conditions and an edge length of 51 particles, reflecting the symmetry of the lattice. At the beginning the (111) surface is covered by a complete layer of randomly distributed  $A$  and  $B$  particles. The concentrations of the adsorbate elements are fixed and denoted as  $\eta_A$  and  $\eta_B$  with  $\eta_A + \eta_B = 1$ .

The system is driven towards thermal equilibrium at temperature  $T$  by means of a rejection-free Monte Carlo method [46, 84]. The precise path towards equilibrium is of no interest here and therefore, we can implement any efficient dynamics, which need not have a realistic microscopic counterpart. Hence, we consider the non-local exchange of one  $A$  and one  $B$  particle on the surface with no limitation on their distance. This results in a significantly faster equilibration than local Kawasaki dynamics [46].

At the beginning the substrate crystal is randomly covered by a complete layer of  $A$  and  $B$  particles of concentrations  $\eta_A$  and  $\eta_B$ , respectively. Then, in every MC step an  $A$  particle at site  $i$  exchanges its binding site with a  $B$  particle at site  $j$ . The pair is selected in each case according to the rates

$$R_{i \rightarrow j} = e^{\frac{\Delta H_i - \Delta H_j}{2kT}} \quad (4.5)$$

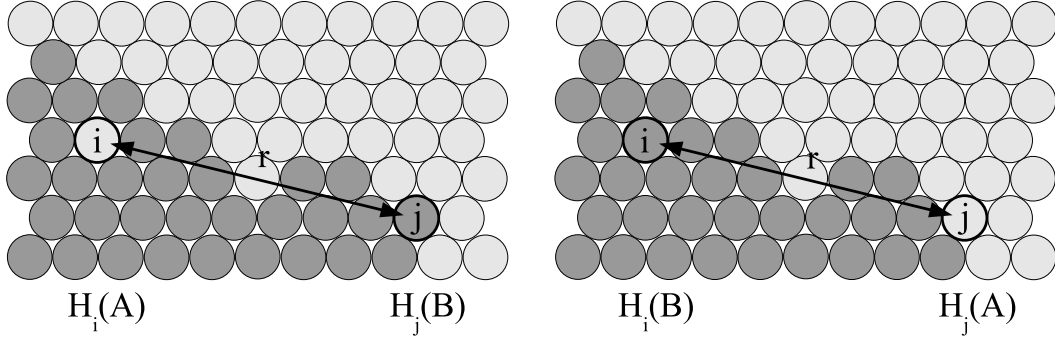


Figure 4.2: Energies for different particles in a distance  $r$  at sites  $i$  and  $j$ . The rate of an exchange event of the two particles depends on the energy differences  $\Delta H_i = H_i(A) - H_i(B)$  and  $\Delta H_j = H_j(A) - H_j(B)$ .

which satisfy the detailed balance condition (2.5). Here  $\Delta H_x = H_x(A) - H_x(B)$  denotes the energy difference of the system with an  $A$  or  $B$  particle at site  $x$ , respectively. Figure 4.2 shows the two configurations of a pair of particles at sites  $i$  and  $j$ . In order to determine  $H_x(A)$  ( $H_x(B)$ ) an  $A$  ( $B$ ) particle is set at the position  $x$  and all particles within the cut-off radius  $r_{cut}$  around  $x$  are relaxed. This state corresponds to a minimum of the total potential energy in the system. The probability for an  $A$  particle on site  $i$  to exchange its site with a  $B$  particle at site  $j$  is given by

$$p_{i \rightarrow j} = p_i^{A \rightarrow B} p_j^{B \rightarrow A} \quad (4.6)$$

with the single probabilities

$$p_i^{A \rightarrow B} = \frac{R_i^{A \rightarrow B}}{\sum_m R_m^{A \rightarrow B}} \quad \text{and} \quad p_j^{B \rightarrow A} = \frac{R_j^{B \rightarrow A}}{\sum_n R_n^{B \rightarrow A}}. \quad (4.7)$$

Here, the rate  $R_i^{A \rightarrow B}$  for a change from  $A$  to  $B$  particle at site  $i$  results from  $R_i^{A \rightarrow B} = e^{\Delta H_i / 2kT}$  if the site is occupied by an  $A$  particle and zero otherwise. Analogously it is essential that  $R_j^{B \rightarrow A} = e^{-\Delta H_j / 2kT}$  if site  $j$  is occupied by a  $B$  particle and zero in other case.

Due to this factorization of probabilities for drawing a site  $i$  occupied by an  $A$  particle and for drawing a site  $j$  occupied by a  $B$  particle in each case a binary tree can be used. Both particle changes are selected according to the probabilities  $p_i^{A \rightarrow B}$  and  $p_j^{B \rightarrow A}$ , respectively. Thus, two binary trees are implemented to select a complete exchange event. To avoid complicated and time-consuming calculations, an exchange process is only permitted if the distance between the involved sites  $i$  and  $j$  is larger than  $r_{cut}$ .

As described in Sec. 3.5 all particles around the two involved sites have to be relaxed after the exchange process is performed. Furthermore, the affected rates

concerning the particles within a distance of  $2r_{cut}$  have to be recalculated.

Hence, the complete algorithm is:

1. The substrate crystal is prepared and covered with a complete layer of randomly distributed adsorbate particles.
2. An exchange event  $A \rightarrow B$  at a site  $i$  is drawn according to its probability  $p_i^{A \rightarrow B}$  and performed.
3. An exchange event  $B \rightarrow A$  at a site  $j$  is drawn according to its probability  $p_j^{B \rightarrow A}$  and performed.
4. The crystal is locally relaxed around the positions of the two particles and the rates of all events affected by the local relaxation are recalculated. The search tree is updated.
5. If the condition for a global relaxation is met the complete system is relaxed and all diffusion rates are recalculated. The search tree is updated.
6. Steps 2 to 5 are repeated until a terminating condition is fulfilled.

After a large enough number of MC steps the system is in equilibrium and the simulation can be stopped.

## 4.2 Influence of model parameters

Naturally, the main question of every simulation is which influence have the particular parameters on the formation of structures. In this context we simulate equilibrium configurations for different misfits, interaction energies, variations of the potential, concentrations of components and temperatures.

### 4.2.1 Misfit and interaction energy

Simulations with various misfit values show that the misfit has, as expected, a strong effect on the structure of surface alloy. Fig. 4.3 shows results for different misfits  $\varepsilon = 0\%$ ,  $5.5\%$ ,  $7.5\%$  (from left to right) at a temperature  $T = 250 K$  after  $10^5$  MC steps. This number of steps is sufficient to reach the equilibrium, see appendix C. The edge length of the hexagon (system size) is set to 51 particles and the energies for interaction between particles of same type are  $E_S = 3.0 eV$  and  $E_A = E_B = 0.5 eV$ , respectively. In the upper row the energy  $E_{AB}$  is set to  $0.35 eV$  and to  $0.45 eV$  in the lower row. In all pictures the larger  $B$  particles are drawn in black in contrast to the smaller  $A$  particles which are gray colored.

Since the misfit is zero the two adsorbate materials are strictly separated in two regions (left column in Fig. 4.3). The reason for this effect is that the

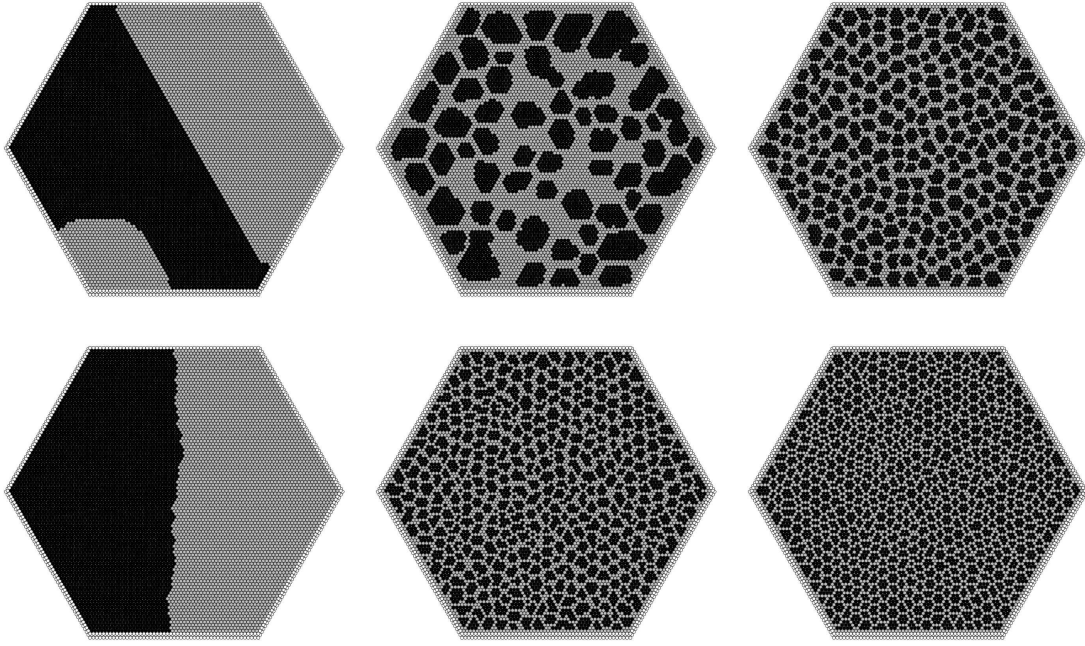


Figure 4.3: Upper row: Simulation results for Lennard-Jones interactions with  $E_{AB} = 0.7 \cdot E_A = 0.35 \text{ eV}$  and  $\varepsilon = 0\%, 5.5\%, 7.5\%$  (from left to right), the particle concentrations are  $\eta_A = \eta_B = 0.5$ . The bigger B particles are shown in black. Lower row: Simulation results for  $E_{AB} = 0.9 \cdot E_A = 0.45 \text{ eV}$ , all other values as above.

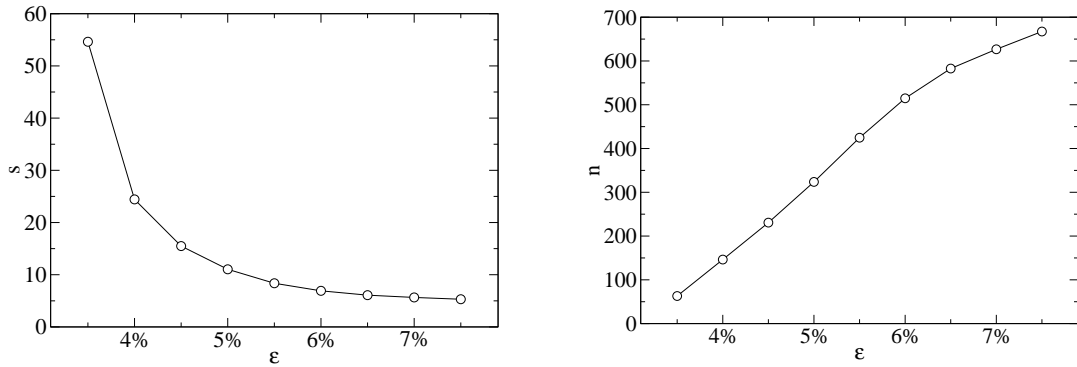


Figure 4.4: Left: The average island size  $s$  consisting of  $B$  particles vs. absolute value of misfit  $\varepsilon$  at the energies  $E_S = 3 \text{ eV}$ ,  $E_A = E_B = 0.5 \text{ eV}$ ,  $E_{AB} = 0.45 \text{ eV}$  and the particle concentrations  $\eta_A = \eta_B = 0.5$ , averaged over three independent simulation runs. Right: The number of islands  $n$  vs. absolute value of misfit  $\varepsilon$  at the same parameters.

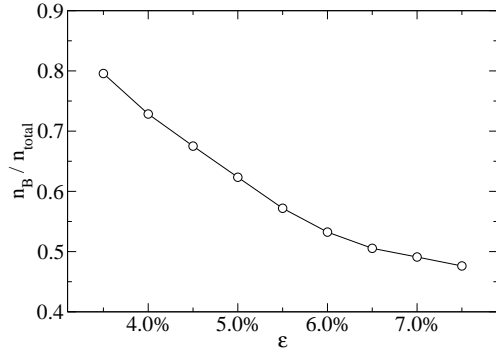


Figure 4.5: The average ratio between the number of neighbor particles of the same type and the total number of neighbor particles vs. the absolute value of misfit  $\varepsilon$  at the energies  $E_S = 3 eV$ ,  $E_A = E_B = 0.5 eV$ ,  $E_{AB} = 0.45 eV$  and the particle concentrations  $\eta_A = \eta_B = 0.5$ , averaged over three independent simulation runs.

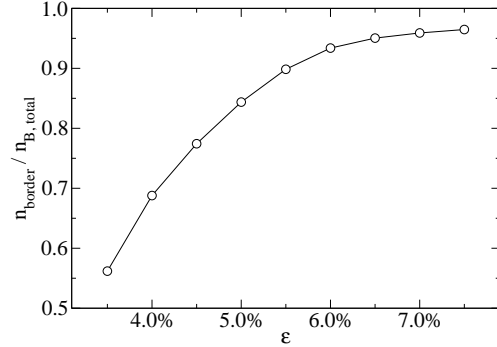


Figure 4.6: The ratio between the number of  $B$  particles at an island border and the total number of  $B$  particles vs. the absolute value of misfit  $\varepsilon$  at the energies  $E_S = 3 eV$ ,  $E_A = E_B = 0.5 eV$ ,  $E_{AB} = 0.45 eV$  and the particle concentrations  $\eta_A = \eta_B = 0.5$ , averaged over three independent simulation runs.

interaction between particles of the same type is stronger than between different particles:  $E_A = E_B > E_{AB}$ . Thus, in this case of no misfit the materials try to find a configuration with minimal number of  $A/B$  nearest neighbor pairs and separation can be observed for all values  $E_{AB} < E_A, E_B$ , if  $\varepsilon = 0$ .

With increasing misfit islands are formed and their number increases with  $\varepsilon$ , see Fig. 4.4. The average size of the islands decreases accordingly. Due to the interaction energy the particles prefer to build one large region of particles of the same type which are located on lattice sites given by the substrate. But due to the positive misfit the  $B$  particles are not able to form a large island and simultaneously to be located at lattice sites. Therefore larger regions of adsorbate  $B$  break apart with increasing misfit and form smaller islands enclosed by  $A$  particles. Larger misfits intensify this effect and more islands are formed.

Fig. 4.5 shows the average ratio between the number of nearest neighbor particles of the same type and the total number of nearest neighbor particles in dependence on the misfit. The graphic demonstrates that the part of neighbor particles of the same material decreases with increasing misfit. This result is analogous to the average island size: if the size of islands decreases the  $B$  particles have accordingly more and more neighbors of adsorbate  $A$ . Simultaneously the number of  $B$  particles which are located at a border of an island increases with increasing misfit, see Fig. 4.6. At smaller islands more  $B$  particles are located next to  $A$  particles.

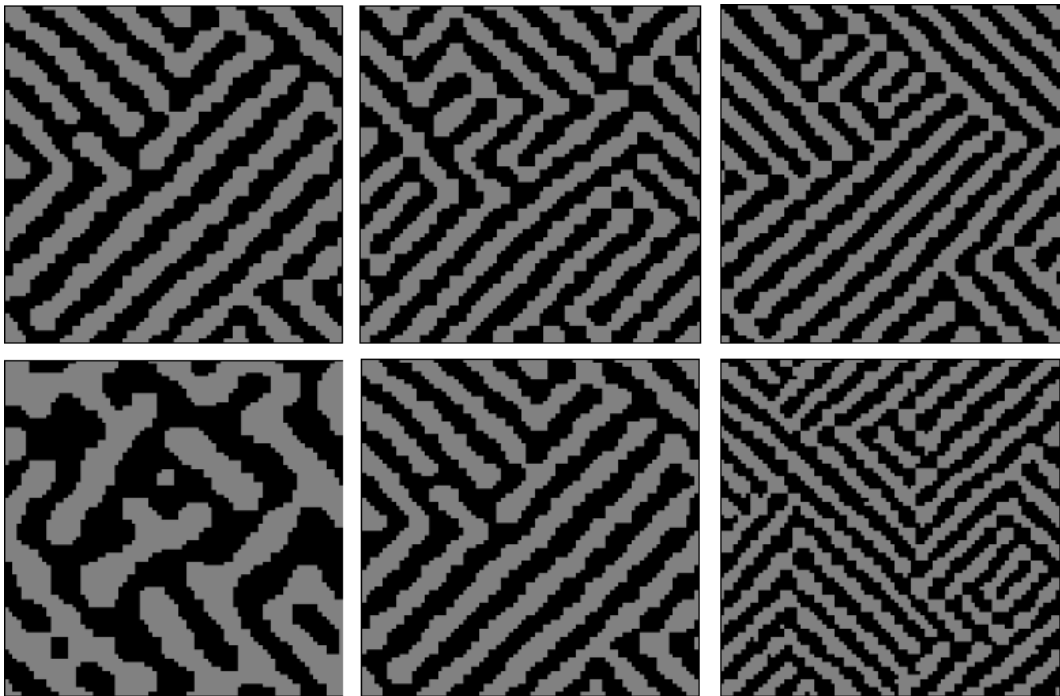


Figure 4.7: Upper row: Snapshots for simple cubic lattice at  $T = 250 K$  with  $E_{AB} = 0.8 E_A$  and  $\varepsilon = 4.5\%, 5.0\%, 5.5\%$  (from left to right). Lower row: Snapshots for simple cubic lattice with  $\varepsilon = 5.5\%$  and  $E_{AB} = 0.6 E_A, 0.8 E_A, 0.9 E_A$  (from left to right). The panels show  $80 \times 80$  sections (Taken from Ref. [56]).

However, the value at which the formation of islands starts depends on the energy  $E_{AB}$ . A larger value of  $E_{AB}$  advances the generation of islands because the interface becomes more and more favorable with stronger interaction between particles of different materials. Therefore, the number of islands increases with increasing  $E_{AB}$  if the misfit is unequal to zero. The smaller  $E_{AB}$ , the more energy it costs to realize boundaries between  $A$  and  $B$  domains and the larger the clusters will be.

Thus, misfit and the energy  $E_{AB}$  have both an essential influence on surface structures. Hence with both parameters the development of islands can be controlled and appropriate combinations result in islands of various size.

A similar behavior has been observed in the case of a simple cubic lattice [14, 56, 85]. However, due to the symmetry stripes instead of islands are formed, see Fig. 4.7. Here, misfit and interaction energy control the stripe width.

So far we considered the case  $E_{AB} < E_A, E_B$ . But if the interaction energy between different adsorbates  $E_{AB}$  is larger than between adsorbates of the same sort  $E_A$  and  $E_B$ , respectively, the situation changes and completely new structures emerge. As Fig. 4.8 shows, in this case stripe-like structures are formed. The



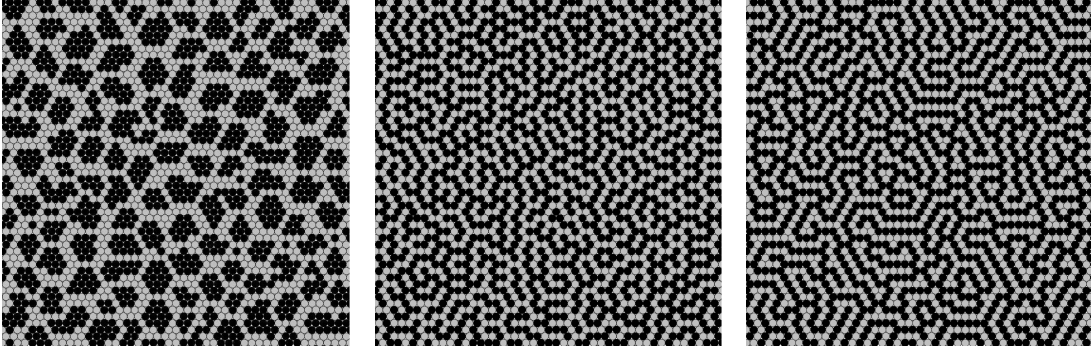


Figure 4.8: Simulation results for Lennard-Jones interactions with  $\varepsilon = 5\%$  and energies  $E_A = E_B = 0.5 eV$  and  $E_{AB} = 0.45 eV, 0.75 eV, 1.50 eV$  (from left to right), the particle concentrations are  $\eta_A = \eta_B = 0.5$ . The panels show 50 x 50 sections, the bigger B particles are drawn in black.

large energy value of  $E_{AB}$  takes care that the number of  $A/B$  nearest neighbor pairs is maximal. Since the concentrations of  $A$  particles and  $B$  particles are equal ( $\eta_A = \eta_B = 0.5$ ) this is realized by stripes. The higher the energy  $E_{AB}$ , the stronger is this effect. Thus, higher energies lead to fewer bendings and more straight stripe sections.

Fig. 4.9 also shows that the form of the stripes is affected by the misfit. Large misfits result in more bendings and fewer straight stripe sections because high misfits prefer having not too many particles in a line. Fig. 4.10 confirms the optical impression. Here, the normalized distribution of the number of straight stripe lengths for various misfits is plotted. The graphic shows the frequency of straight parts of particle chains (sections without a bend), independent of the direction of these straight lines. Lower misfits lead to more straight segments in contrast to higher values, for which more bendings and hence shorter straight segments are favored.

This formation is again a consequence of the competition between misfit and particle location on lattice sites and originates from the fact that, for high positive misfits, particles which are jammed between two neighbors of the same type try to sidestep and build a bend. Hence, a meandering configuration has less strain and becomes more favorable for increasing misfit.

## 4.2.2 Interaction potential

So far we considered Lennard-Jones potentials with exponents  $n = 12$  and  $m = 6$ . But we also studied generalized  $n, m$  potentials with other exponents according

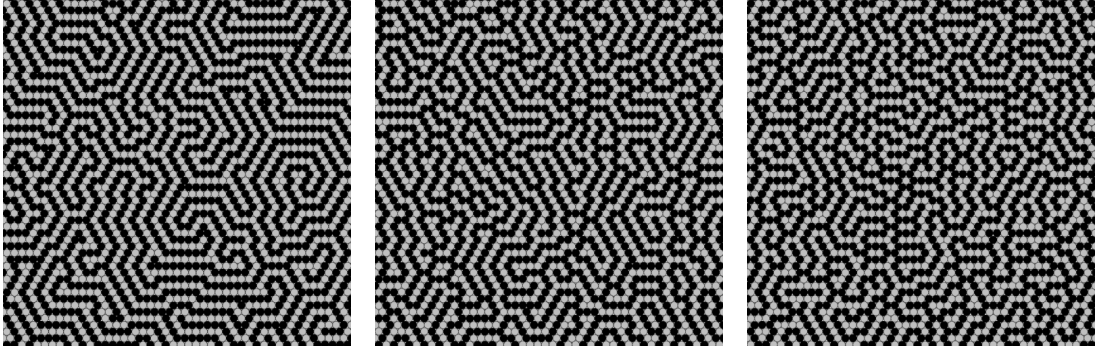


Figure 4.9: Simulation results for Lennard-Jones interactions with  $E_A = E_B = 0.5 eV$ ,  $E_{AB} = 1.5 eV$  and  $\varepsilon = 1\%, 4\%, 7\%$  (from left to right), the particle concentrations are  $\eta_A = \eta_B = 0.5$ . The panels show  $50 \times 50$  sections, the bigger B particles appear in black.

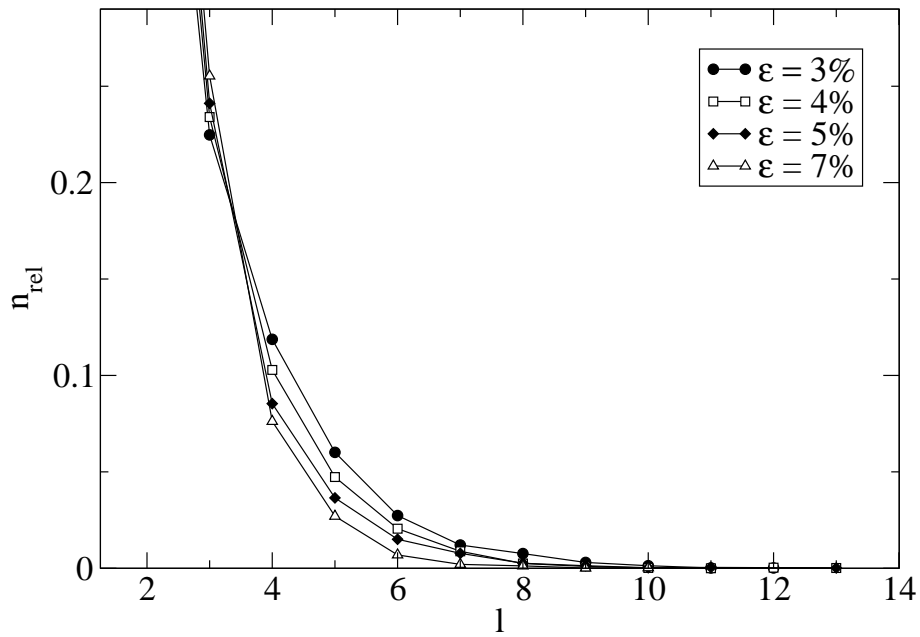


Figure 4.10: Relative number  $n_{rel} = n/n_{total}$  of straight stripe lengths  $l$  in the system for different misfits, other parameters as in Fig. 4.9.

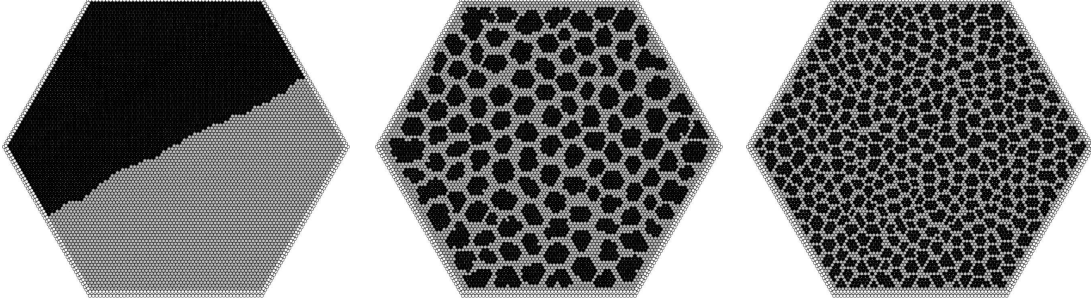


Figure 4.11: Surfaces for a modified Lennard-Jones potential with exponents  $n = 10.5$  and  $m = 6$ . The parameters are  $E_A = E_B = 0.50 \text{ eV}$ ,  $E_{AB} = 0.40 \text{ eV}$  and  $\varepsilon = 0\%, 5.5\%, 7.5\%$  (from left to right), the particle concentrations are  $\eta_A = \eta_B = 0.5$ .

to

$$U(r_{ij}) = E_{ij} \left[ \frac{m}{n-m} \left( \frac{r_{ij}^0}{r_{ij}} \right)^n - \frac{n}{n-m} \left( \frac{r_{ij}^0}{r_{ij}} \right)^m \right] \quad (4.8)$$

with  $n > m$  [86, 87], see also Appendix A. By variation of the exponents more realistic interactions can be implemented, examples for different metals are given in [87]. Simulations with  $n \neq 12$  and  $m \neq 6$  lead to very similar results as the 12, 6 Lennard-Jones potential, but the computational effort strongly increases. As an example, Fig. 4.11 shows surfaces in simulations with  $n = 10.5$  and  $m = 5.5$ . The qualitative findings do not depend on the detailed properties of the potential considered and persist for a large variety of interactions.

### 4.2.3 Concentration of components

The variation of concentrations of the adsorbate components has essential consequences on the formation of alloy structures. In the simulations presented up to now the used concentrations have been  $\eta_A = \eta_B = 0.5$ . By contrast, Fig. 4.12 displays surfaces with interaction energies  $E_{AB} < E_A, E_B$ , but different  $A$  particle concentrations  $\eta_A = 0.3, 0.5$  and  $0.7$ . The snapshots show that the average island size changes with the adatom concentrations.

This effect can be quantified by calculating the average  $B$  island sizes and the according number of  $B$  islands, see Fig. 4.13. The diagram on the left hand side shows the average island size consisting of  $B$  particles, the diagram on the right hand side the according number of islands. Small concentrations of  $A$  particles  $\eta_A$  lead to big  $B$  islands, because the  $B$  particles have to form large clusters as a result of their superior number. With increasing  $\eta_A$  the average island size decreases, but for large concentrations of  $A$  particles the islands of  $B$  particles becomes only slightly smaller. So, for high values of  $\eta_A$  the average size depends

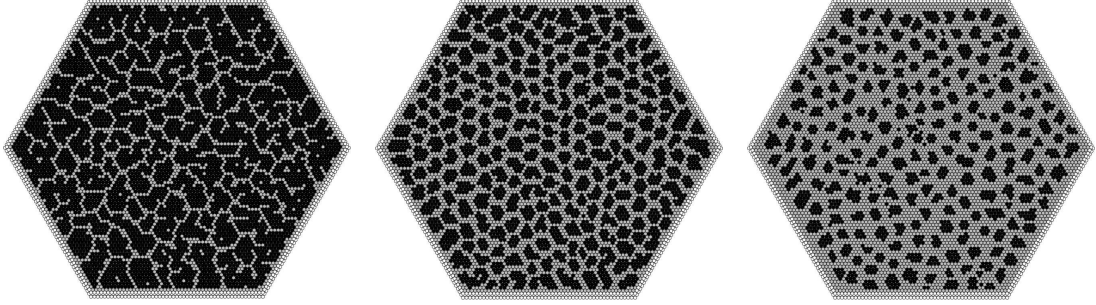


Figure 4.12: Surfaces for  $\eta_A = 0.3, 0.5, 0.7$  (from left to right). The other parameters are  $E_A = E_B = 0.50 \text{ eV}$ ,  $E_{AB} = 0.45 \text{ eV}$  and  $\varepsilon = 4.5\%$ .

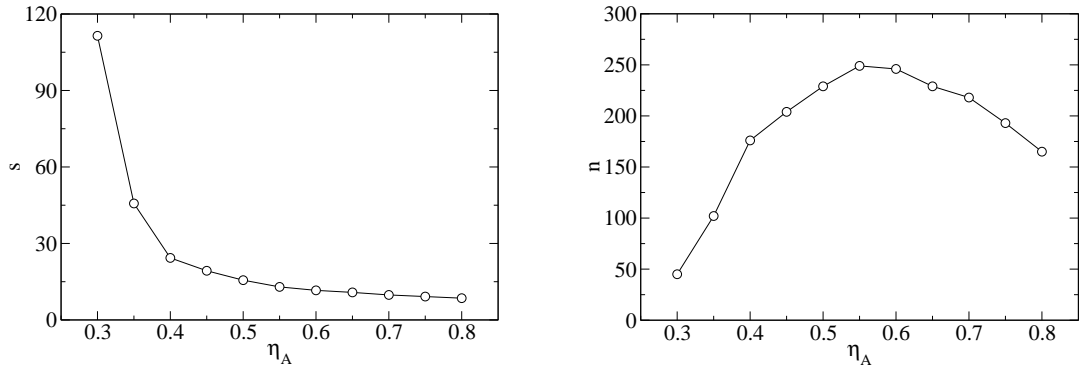


Figure 4.13: Left: The average island size  $s$  consisting of  $B$  particles vs. the concentration of  $A$  particles  $\eta_A$  at the energies  $E_S = 3 \text{ eV}$ ,  $E_A = E_B = 0.5 \text{ eV}$ ,  $E_{AB} = 0.45 \text{ eV}$  and misfit  $\varepsilon = 4.5\%$ . Right: The number of  $B$  islands  $n$  vs. the concentration of  $A$  particles  $\eta_A$  at the same parameters.

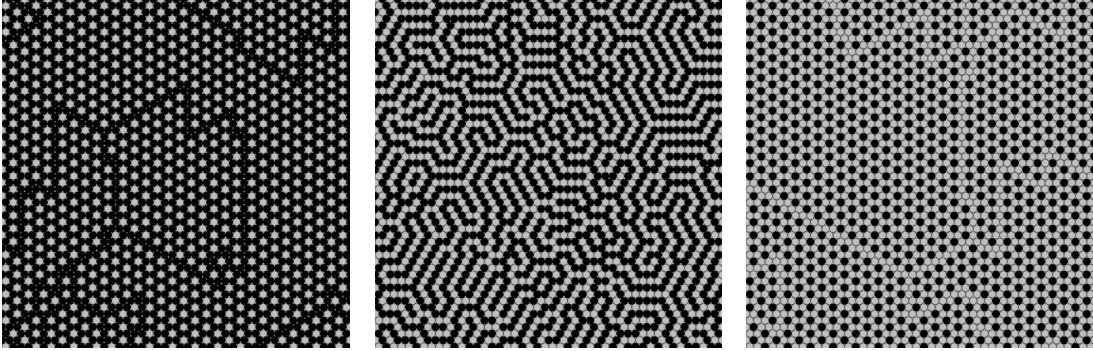


Figure 4.14: Simulation results for Lennard-Jones interactions with particle concentrations  $\eta_A = 0.3, 0.5, 0.7$  (from left to right), the other parameters are  $E_A = E_B = 0.5 \text{ eV}$ ,  $E_{AB} = 0.75 \text{ eV}$ ,  $\varepsilon = 1\%$  and  $T = 250 \text{ K}$ . The panels show  $50 \times 50$  sections, the bigger B particles appear in black.

only weakly on the concentration.

On the contrary, the number of  $B$  islands has a maximum at a concentration  $\eta_A \approx 0.55$ . For low values the number increases with increasing  $\eta_A$  according to the average island size, until a maximum is reached, and for higher concentrations the island number decreases again. The reason for this is the decreasing number of  $B$  particles: at a certain point there are not enough  $B$  particles in the system to build enough islands of the favored size and therefore the number of islands decreases.

In addition, the average distance between  $B$  islands changes with  $\eta_A/\eta_B$ . With decreasing number of islands their distances increase more and more, so that the islands are dispersed over the whole crystal.

If the interaction between particles of different material is stronger than that between particles of the same material,  $E_{AB} > E_A, E_B$ , the variation of the particle concentration from a low to a high value leads to an interesting evolution of patterns. Fig. 4.14 illustrates the effect for three different concentrations  $\eta_A = 0.3, 0.5, 0.7$  with  $E_{AB} = 0.75 \text{ eV} > E_A = E_B = 0.5 \text{ eV}$ , misfit  $\varepsilon = 1\%$  and temperature  $T = 250 \text{ K}$ . At low concentrations of the smaller  $A$  adatoms, each of them is surrounded by neighbors of  $B$  type only. For slightly larger  $\eta_A$ , short linear clusters of  $B$  atoms begin to form, and for  $\eta_A \approx \eta_B$  we observe stripe formation all over the system cf. Fig. 4.14 (center panel). Finally, a high concentration of  $A$  particles leads to the formation of structures which are similar to the case of small  $\eta_A$ , but with the role of  $A$  and  $B$  exchanged. In addition, one can recognize the formation of line defects at the right and the left panels dominated by particles of different type respectively. Qualitatively, the behavior resembles the evolution from 2D droplets to inverted 2D droplets during deposition of Pb on Cu(111) investigated in [88–90].

For concentrations between  $\eta_A = 0.5$  and  $\eta_A = 0.66$  the particles with positive

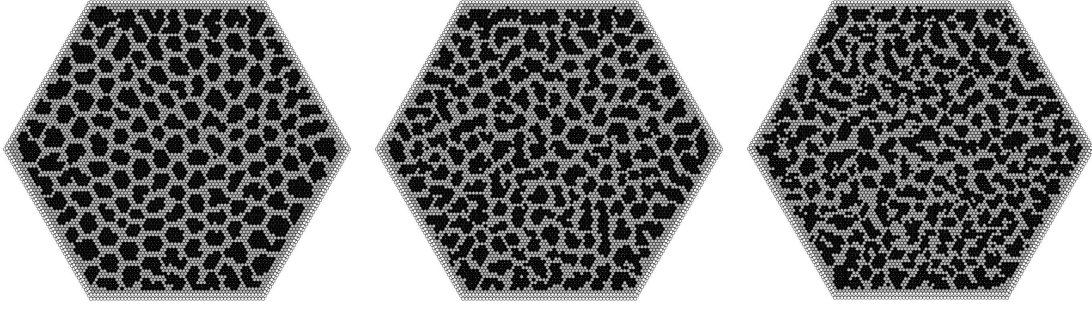


Figure 4.15: Surfaces for different temperatures  $T = 200 K, 400 K, 600 K$  (from left to right). The other parameters are  $E_A = E_B = 0.50 eV$ ,  $E_{AB} = 0.45 eV$ ,  $\varepsilon = 4.0\%$  and  $\eta_A = \eta_B = 0.5$ .

misfit tend to form small islands with a few particles in a row. The emerging small stripe-like shaped islands are evenly dispersed over the whole system. In this case some structures are very similar to  $\text{Pd}_{0.72}\text{Au}_{0.28} / \text{Ru}(0001)$  systems studied in [19].

#### 4.2.4 Temperature

The temperature has also an influence on the pattern formation. Fig. 4.15 shows the change of island forms with temperature. At low temperatures the islands are quite compact, but with increasing temperatures their structures meander more and more, and the islands are rather elongated at higher temperatures.

However, number and size of islands depend only weakly on the temperature in the observed interval, see Fig. 4.16. Only at temperatures higher than  $400K$  the fluctuations increase and a very small trend is visible: the average island size increases a little bit and accordingly the number of islands decreases.

In Fig. 4.17 the average ratio between the number of neighbor particles of the same type and the total number of neighbor particles in dependence on the temperature is plotted. The part of  $B$  particles slightly decreases with increasing temperature. This confirms the optical impression that the islands change their shape, and the compact forms meander at higher values of  $T$  to ramified islands. This effect becomes more evident in Fig. 4.18. The graphic shows the ratio between the number of  $B$  particles, which are located at an island border, and the total number of  $B$  particles in dependence on the temperature. The curve progression demonstrates that more and more  $B$  particles become border particles with increasing  $T$  and proves obviously the changing island shapes.

In the case of  $E_{AB} > E_A, E_B$ , the form of stripes depends also on the temperature as Fig. 4.19 illustrates. An increase of the temperature leads to a similar effect as an increase of the misfit: At low temperatures the average length of straight stripe sections is larger than at higher temperatures. Fig. 4.20 shows

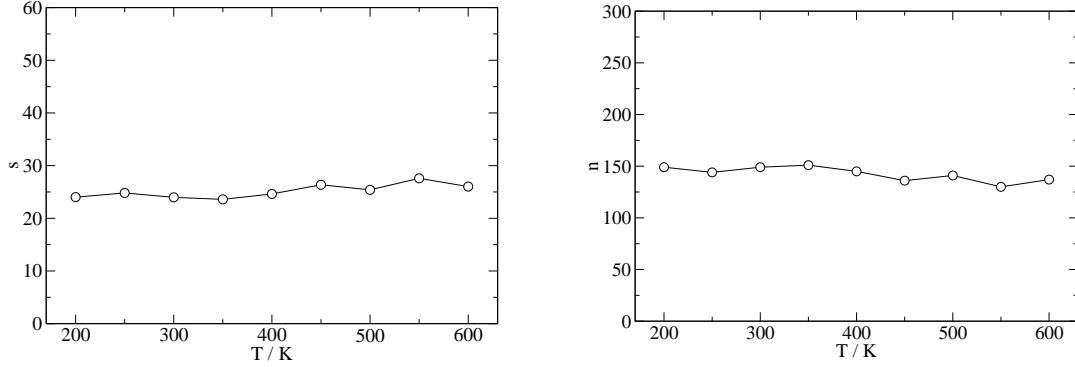


Figure 4.16: Left: The average island size  $s$  consisting of  $B$  particles vs. the temperature  $T$  at the energies  $E_S = 3 eV$ ,  $E_A = E_B = 0.5 eV$ ,  $E_{AB} = 0.45 eV$ , misfit  $\varepsilon = 4.0\%$  and concentrations  $\eta_A = \eta_B = 0.5$ . Right: The number of  $B$  islands  $n$  vs. the temperature  $T$  at the same parameters.

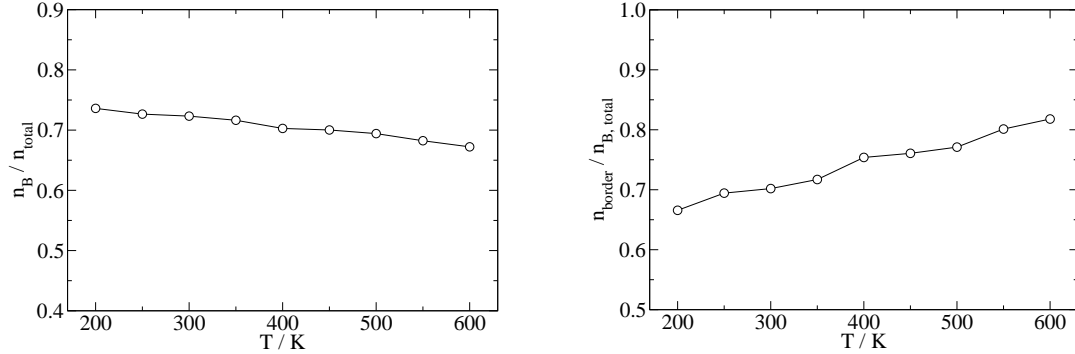


Figure 4.17: The average ratio between the number of neighbor particles of the same type and the total number of neighbor particles vs. the temperature  $T$  at the energies  $E_S = 3 eV$ ,  $E_A = E_B = 0.5 eV$ ,  $E_{AB} = 0.45 eV$ , misfit  $\varepsilon = 4.0\%$  and concentrations  $\eta_A = \eta_B = 0.5$ .

Figure 4.18: The ratio between the number of  $B$  particles at an island border and the total number of  $B$  particles vs. the temperature  $T$  at the energies  $E_S = 3 eV$ ,  $E_A = E_B = 0.5 eV$ ,  $E_{AB} = 0.45 eV$ , misfit  $\varepsilon = 4.0\%$  and concentrations  $\eta_A = \eta_B = 0.5$ .

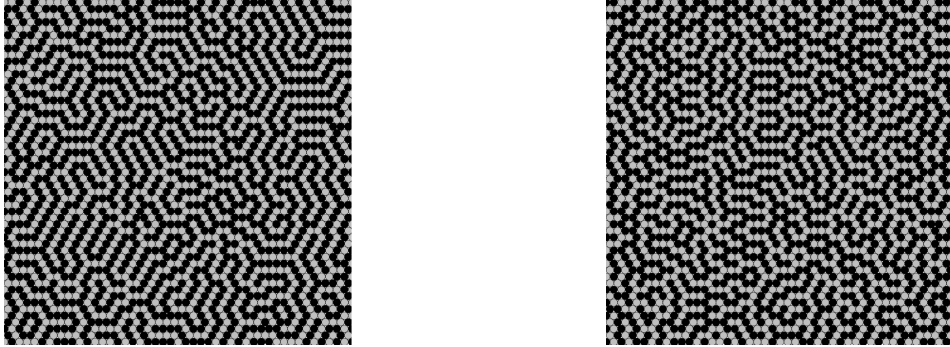


Figure 4.19: Surfaces for  $T = 250\text{ K}$  (left) and  $600\text{ K}$  (right). The other parameters are  $E_S = 3.00\text{ eV}$ ,  $E_A = E_B = 0.50\text{ eV}$ ,  $E_{AB} = 0.75\text{ eV}$ ,  $\varepsilon = 1\%$  and  $\eta_A = \eta_B = 0.5$ .

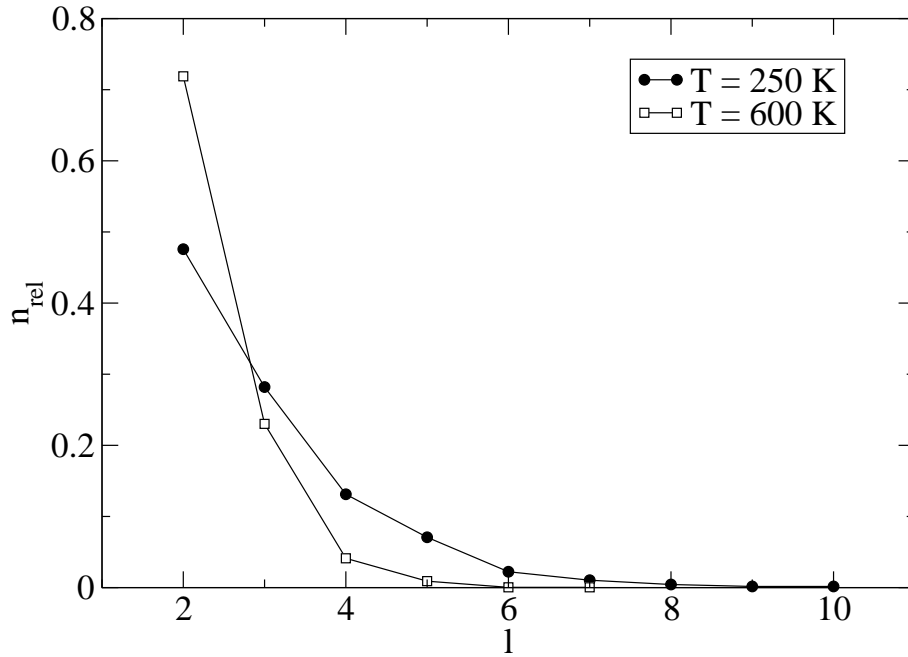


Figure 4.20: Relative number  $n_{rel} = n/n_{total}$  of straight stripe lengths  $l$  in the system for different temperatures. The other parameters are as above.



the normalized distribution of the number of straight stripe lengths for different temperatures. In contrast to low temperatures high values result in more bendings and fewer straight sections and the structures are evocative of high misfits. Thus, also in the case of  $E_{AB} > E_A, E_B$  a meandering effect can be observed, if the temperature increases.

## 4.3 Conclusions

In this chapter we have presented simulation results for systems in thermal equilibrium. For this purpose we reconstructed an fcc crystal with three fixed bottom layers. At the beginning the substrate was randomly covered with one layer of adsorbate particles of two different materials and afterwards the system was driven towards thermal equilibrium by using a rejection-free Monte Carlo method.

It was shown that the variation of misfit and interaction energies  $E_{AB}$  leads to different numbers of islands and different average island sizes. Thus, surface confined alloying is a possible strain relaxation mechanism. Increasing misfit just as large values of  $E_{AB}$  result in small islands of  $B$  particles. If the interaction between different adsorbate species is even stronger than that between same species,  $E_{AB} > E_A, E_B$ , stripe-like structures are formed. However, the detailed forms of the stripes are influenced by the misfit. The time consuming use of generalized Lennard-Jones potentials with exponents  $n \neq 12$  and  $m \neq 6$  yield very similar results as the computationally advantageous 12,6 potential.

The variation of particle concentrations also has an influence on the emerging structures. A small concentration of  $A$  particles leads to the formation of only a few big  $B$  islands, but with increasing  $\eta_A$  the average island size decreases. However, for high concentrations of adsorbate  $A$  the size varies only weakly. If  $E_{AB} > E_A, E_B$  at low concentrations of one sort single islands of this material are formed. The evolution from low to high concentrations resembles qualitatively the evolution from 2D droplets to inverted 2D droplets observed e.g. in experimental studies of Pb / Cu(111) systems [88–90].

Different temperatures indeed hardly change the number of formed islands, but the temperature controls the shape of the islands. Higher values result in more meandering structures with ramified islands.

Due to the self-organization of the involved particles, promising nanostructures could be produced just by controlling the parameters. In this context the pattern formation for further lattices in equilibrium simulations can be of interest. Therefore, it is necessary to investigate the behavior of ternary systems with other realistic lattice symmetries. Another interesting point is the use of more realistic potentials, like e.g. empirical bond order incorporating potentials [91,92] or tight-binding potentials [93].



# Chapter 5

## Growth simulations

In the last chapter we have presented which structures are built on the surface if the system is in equilibrium. In this chapter we investigate how structures are emerging in the first adsorbate monolayer onto the substrate.

Similar to the case of equilibrium, alloying structures can be formed to reduce strain in growth simulations of ternary systems with two adsorbate materials. Strain relaxation and kinetic segregation are also the two main mechanisms leading to energetically favorable configurations. In this context the calculation of different energy barriers for various parameters is of particular interest. Here, an important point is how the activation barriers and the resulting structures are influenced by the different parameters like interaction energy or misfit.

For simulating epitaxial growth the particular processes, which are playing the essential role, have to be implemented. In the first section we describe the model used in our simulations and how the processes are realized. After that we present some results of the Kinetic Monte Carlo (KMC) simulations and draw a comparison to the equilibrium simulations of the previous chapter.

### 5.1 The growth model

The main goal is to investigate the influence of different parameters on the growth and the structure formation. For that purpose we use a basic setup similar to that of the equilibrium simulations as introduced in Sec. 4.1. At the beginning of the simulation an fcc crystal consisting of substrate particles is constructed and the interactions of all particles in the simulations are realized by the 12,6 Lennard-Jones potential, which is cut off at the distance  $r_{cut} = 3r_s^0$ .

However, the simulation of realistic growth processes needs another approach than in the case of equilibrium simulations. Therefore we use an off-lattice Kinetic Monte Carlo method to realize the growth dynamics. As in the equilibrium simulations every event gets a certain rate and all rates are saved in a binary tree. But in contrast to the equilibrium simulations only one binary tree is necessary

and each event therein represents a realistic microscopic process.

### 5.1.1 Off-lattice Kinetic Monte Carlo simulations

In every simulation step one event from the binary tree is drawn. Since desorption is neglected the only possible mechanisms are deposition and diffusion.

The deposition event occurs with a certain rate  $R_d$  and the sort of the deposited particle is chosen with a probability of  $p_A$  for adsorbate  $A$  and  $p_B$  for adsorbate  $B$ . The deposition rate depends on the flux which reaches the surface. In binary systems only one adsorbate is deposited and accordingly  $p_A$  or  $p_B$ , respectively, is set to 1, while the other value is zero. By contrast in ternary systems the probabilities are in general chosen as  $p_A = p_B = 0.5$ .

If a deposition event is drawn, a new adsorbate particle, which is arriving at the crystal surface, is set on a random free position on the substrate and then the adatom is positioned at the next energetic favorable binding site by local relaxation. After that the rates of all particles in the neighborhood have to be recalculated and the binary tree has to be updated.

The rate of a diffusion event depends on the activation energy which results from the binding energy and the energy at the saddle point, see Sec. 3.4. Therefore it is evident that for every possible diffusion process the saddle point has to be determined.

Naturally for every new configuration the activation energies and the according rates of the affected region have to be recalculated and the binary tree has to be updated, so that all events are drawn with the correct probability.

### 5.1.2 Ball and spring model

An disadvantage of the off-lattice Kinetic Monte Carlo method described in the last section is the enormous computational effort for calculating the saddle points. In many cases this slows down the simulation heavily and a simplification is necessary to obtain significant results.

An idea adumbrated in Sec. 3.4 is to use a ball and spring like method for determining the energy at the transition state without calculating the exact position of the saddle point. In this method the number of occupied nearest and next-nearest neighbors is counted and with this information the energy at the saddle point is estimated. For that purpose energies at the correct saddle points are measured by using the activation-relaxation technique for different configurations and parameters and a catalogue is set up. This list can be used for getting the approximate energy at the transition site between two binding sites in the growth simulations.

In contrast to the pure ball and spring model, as used e.g. in [67], the energy at the binding site is calculated exactly. This approach allows a faster simulation

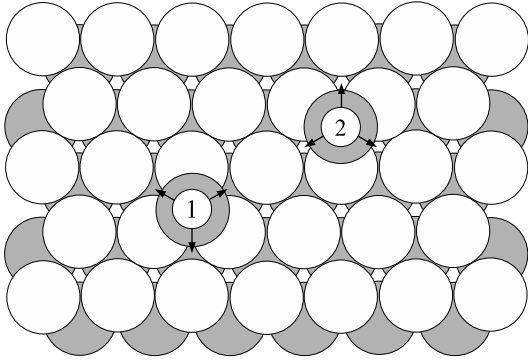


Figure 5.1: Top view on an fcc surface: Particle 1 located on an fcc site has three possible neighboring sites (all are hcp sites) to which it can jump. Particle 2 positioned on a hcp site can attain one of the three adjacent fcc sites.

than in the case of an exact calculation of the saddle point energies, but yields more precise values of the activation energies than pure ball and spring.

## 5.2 Energy barriers

Since the rates of all diffusion events depend on the energy barriers the study of these barriers is of particular interest. Thus the energy barriers control the dynamics and, consequently, the formation of structures in epitaxy. In this context the main question is how different parameters influence the energy values.

In principle every particle on an fcc surface may be located on an fcc or a hcp site. Both positions are binding sites resulting from the lattice as demonstrated in Sec. 3.1. During the growth process an adatom jumps from an fcc site to a hcp site or vice versa, respectively, because every fcc site is surrounded only by hcp sites and every hcp site only by fcc sites. Fig. 5.1 illustrates this fact. Since the adatom diffuses on the flat surface without any islands or step edges it has three adjacent sites to which it can jump.

### 5.2.1 Diffusion on plane surfaces

Due to its essential effect on the growth behavior the influence of the misfit on the energy values is a subject which is worthwhile to study. Therefore we deal at first with the interesting question how the binding energies and diffusion barriers on the plane substrate surface depend on the misfit.

Fig. 5.2 shows the binding energy  $E_b$  of an isolated particle placed on an fcc site in dependence on the misfit. The bigger the misfit the stronger is the binding to the surface and the binding energy constantly decreases with increasing misfit. Similar results with decreasing energy are presented in [94–98]. The transition energy  $E_t$  displayed in Fig. 5.3 shows a very similar behavior. Here, the saddle point is determined by ART. The diffusion barrier resulting from transition energy and binding energy,  $E_a = E_t - E_b$ , also decreases linearly with increasing  $\varepsilon$ , as it is demonstrated in Fig. 5.4.

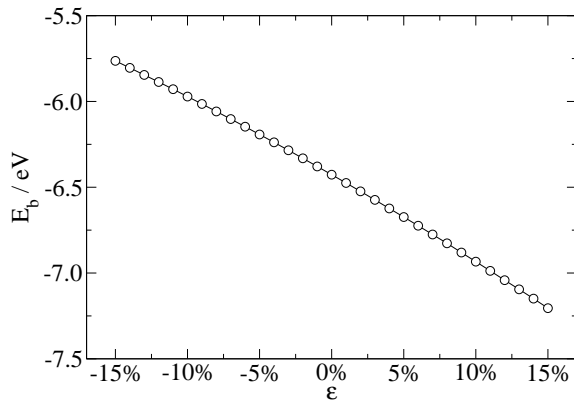


Figure 5.2: Binding energy of a particle on an fcc site on the plane surface vs. misfit. The interaction energies in the used Lennard-Jones 12,6 potential are  $E_S = 3.00 \text{ eV}$  and  $E_A = 0.50 \text{ eV}$ .

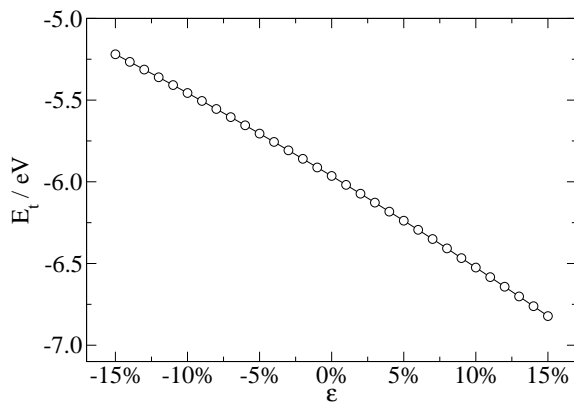


Figure 5.3: Transition state energy of a particle on an fcc site vs. misfit. The interaction energies are the same as above.

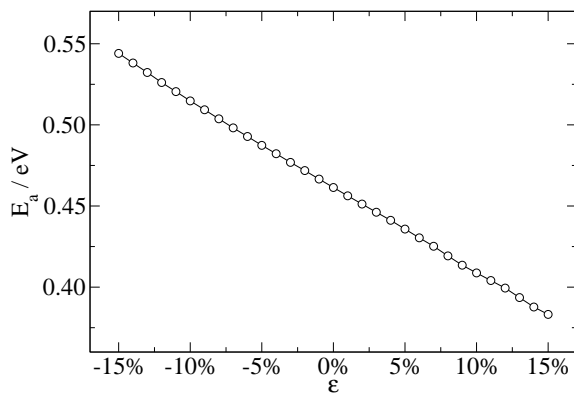


Figure 5.4: Diffusion barrier of a particle on an fcc site vs. misfit. The interaction energies are the same as above.

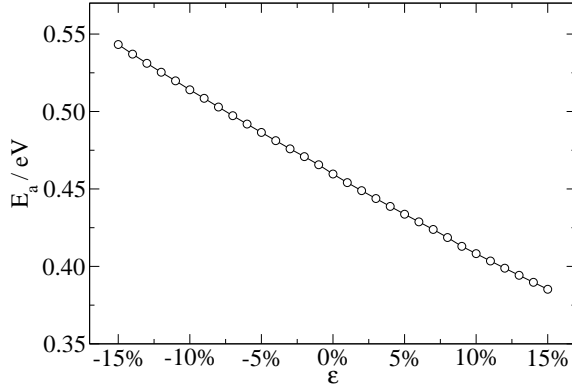


Figure 5.5: Diffusion barrier of a particle on a hcp site vs. misfit. The interaction energies are the same as above.

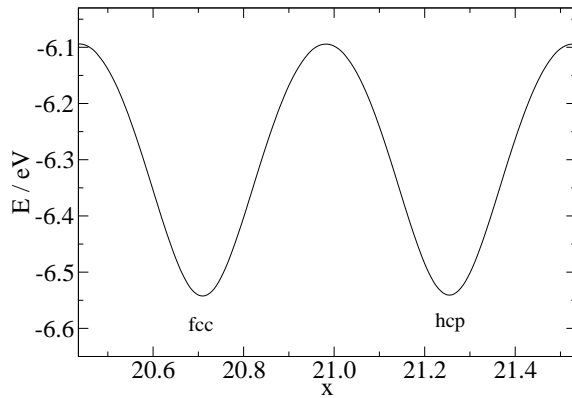


Figure 5.6: Potential energy for a test particle diffusing on the surface in direction of the x axis. The misfit is  $\epsilon = 3\%$ .

The behavior on hcp sites is the same: both binding and transition state energy decrease with increasing misfit. The activation energy for a diffusion event from a hcp to an fcc site is plotted in Fig. 5.5, the curve progression is almost the same as in the case of fcc site described before.

In this context it is noticeable that an adatom on an fcc site and an adatom on a hcp site have almost the same binding energy. The value on an fcc site is a little bit lower, but the difference between the two sites is very small:  $\Delta E(fcc-hcp) \approx 2 \text{ meV}$ . Fig. 5.6 shows the potential energy for a test particle diffusing on the surface in direction of the x axis. The two minima in the curve represent the fcc and the hcp site having almost the same energy. The maximum in the figure separating the two binding sites corresponds to the saddle point in the three-dimensional PES. Thus, there is nearly no energetic preference for fcc sites on the surface of the fcc substrate crystal.

In experimental and theoretical studies it is shown that it depends on the used materials which site is preferred. In the case of Cu on Cu(111) [99], Pt on Pt(111) [100], and Ag on Al(111) [101] an fcc site preference was found, in the case of Ir, Re, and W on Ir(111) and Al on Al(111) [102] it is determined single adatoms to be located on hcp sites [103, 104]. A rule predicting the site preference was developed for metals having a partly filled *d* band [105]. Another aspect which has an influence on the favored site is the cluster size of adatoms, as

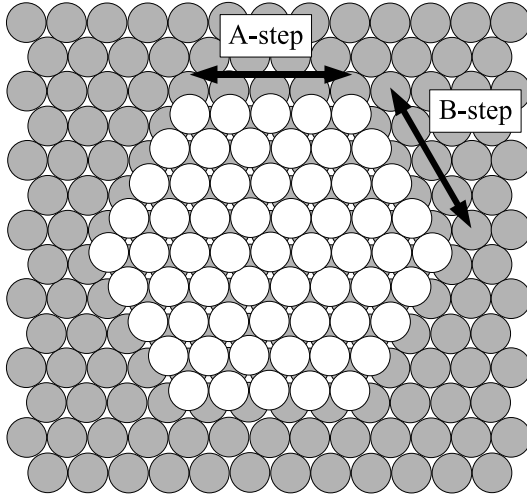


Figure 5.7: Top view of an island placed on an fcc(111) surface with the two characteristic kinds of step edges A and B.

was demonstrated for Ir/Ir(111) [106]. Nevertheless, in most cases the difference of the binding energies is very small for single adatoms and the particles can occupy the fcc as well as the hcp site. The dynamics of jumps out of fcc versus hcp sites are much the same. Thus, the results in our simulations are comparable with experimental behavior.

### 5.2.2 Barriers at step edges

Another point to be considered are the energy barriers at step edges. There are two different kinds of island edges on an fcc(111) surface, see Fig. 5.7. The illustration shows so-called A-steps which form  $\{100\}$  microfacets at the step edge and B-steps corresponding to  $\{111\}$  microfacets. Due to the different configurations different diffusion behaviors can be observed at the different edges [22,96,107,108]. In order to investigate the growth behavior it is of particular interest to study barriers at different edges and positions at the island.

For such investigations we constructed a hexagonal island on the substrate and set a particle of the same type at the step edge. In Fig. 5.8 the binding energy of

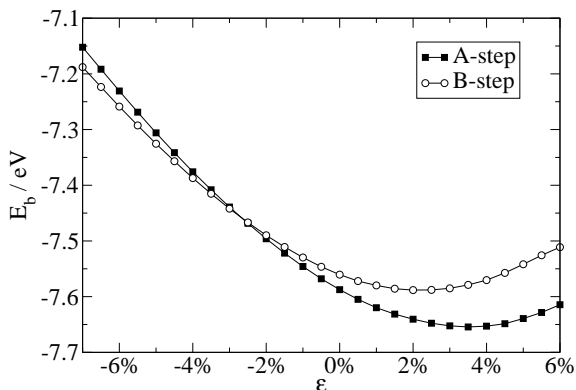


Figure 5.8: Binding energy of a particle positioned at a step edge vs. misfit. The interaction energies in the used Lennard-Jones 12,6 potential are  $E_S = 3.00 \text{ eV}$  and  $E_A = 0.50 \text{ eV}$ .



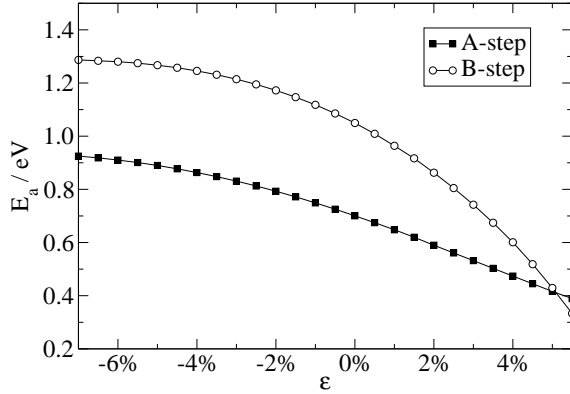


Figure 5.9: Diffusion barrier of a particle positioned at a step edge vs. misfit. The interaction energies are the same as in Fig. 5.8.

the particle in dependence on the misfit is plotted. The curves for a position at an A-step and for a position at a B-step show a very similar progression. Since the misfit is negative the behavior is the same as on a plane surface and the binding energy decreases with increasing misfit. However, at a certain value of  $\epsilon$  a minimum is reached and the binding energy begins to increase.

The reason for that behavior is that the island expands with increasing positive misfit and pushes the single particle into an energetic less favorable position. At a certain value this effect is stronger than the effect of decreasing energy detected on a plane surface and the binding energy increases. In the studied system the minimum is at about  $\epsilon = 3.5\%$  in the case of an A-step and at about  $\epsilon = 2.0\%$  in the case of a B-step.

The diffusion barriers decrease with increasing misfit as shown in Fig. 5.9 for an A-step and for a B-step, respectively. In the first case the energy barrier for a jump weakly decreases at the beginning and begins to diminish almost linearly at  $\epsilon \simeq -2.0\%$ . At the B-step the curve is smooth at the beginning and crosses over to a parabola with increasing misfit. For values of  $\epsilon \gtrsim 5\%$  the barriers at B-steps are smaller than at A-steps.

At  $\epsilon \simeq 5.5\%$  for an A-step and at  $\epsilon \simeq 5.0\%$  for a B-step, respectively, the barrier becomes smaller than that on the plane surface and step edge diffusion becomes more favorable in energetic respect. A similar effect is observed in a simulation of growth on a bcc(100) surface [98].

### 5.3 Influence of misfit and interaction energy

In the following we present and discuss results obtained in off-lattice KMC simulations. The calculation of saddle point energies by means of ART would be very time consuming, and to keep the times of our growth simulations within a feasible limit we use the ball and spring like model described in Sec. 5.1. Since we are only interested in the submonolayer regime, we ignore particles deposited onto other particles and jumps of particles onto others are suppressed.

As in the case of equilibrium the attempt frequency is set to  $\nu_0 = 10^{12} \text{ Hz}$

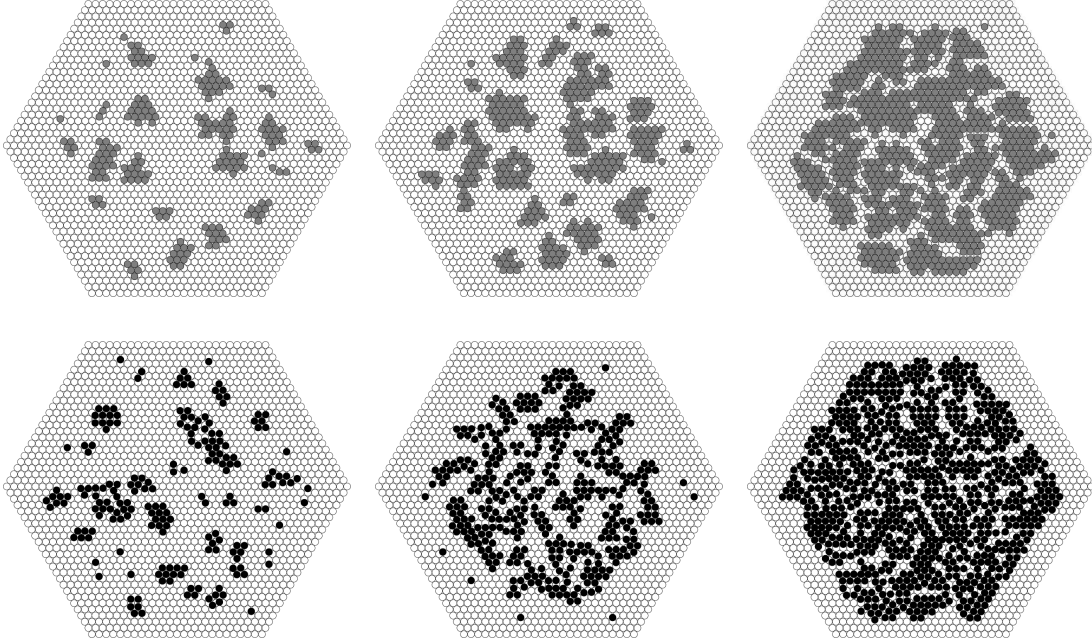


Figure 5.10: Upper row: Simulation results for Lennard-Jones interactions with  $E_S = 3.00 \text{ eV}$ ,  $E_A = 0.75 \text{ eV}$ , and  $\varepsilon = -5.0\%$  with  $n = 200, 400, 800$  adsorbate particles (from left to right). The temperature is set to  $T = 700 \text{ K}$  and the deposition rate to  $R_d = 0.0005 \text{ ML/s}$ . Lower row: Simulation results for  $\varepsilon = +5.0\%$ , all other parameters are the same.

for all simulation runs. Unless otherwise mentioned the temperature is chosen as  $T = 700 \text{ K}$ , the edge length of the hexagon (system size) as 25 particles and the deposition rate as  $R_d = 0.0005 \text{ ML/s}$  for each type of adsorbate.

### 5.3.1 Binary systems

At first we consider a system with only one adsorbate. The upper row of Fig. 5.10 shows the formation of particles with negative misfit  $\varepsilon = -5.0\%$ . The interaction energies in the Lennard-Jones potential are set to  $E_S = 3.00 \text{ eV}$  and  $E_A = 0.75 \text{ eV}$ , respectively.

The three pictures of different stages of development clearly illustrate the process of coarsening. In the beginning of the simulation only few particles exist, which form small compact islands. Since the binding energies on fcc and hcp sites have almost the same value, islands both on fcc and hcp sites emerge. In further progression more and more adatoms are deposited and the size of the islands increases. As a consequence the islands merge to larger islands, until finally only one large island exists.

Another point to be considered is that the value of misfit affects a lot the formation of structures. At lower absolute values of misfit the adsorbate tends

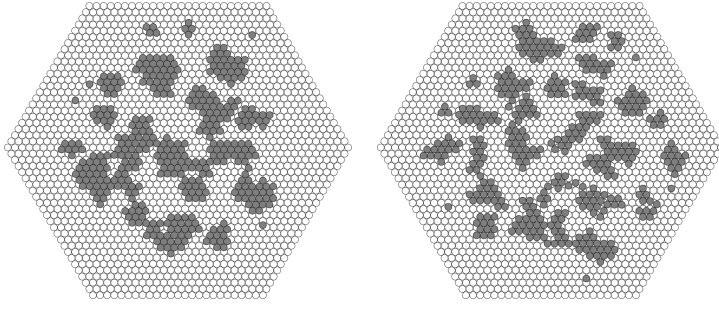


Figure 5.11: Surfaces with 400 adsorbate particles at  $\varepsilon = -7.0\%$  (left) and  $\varepsilon = -1.0\%$  (right). All other parameters are as in Fig. 5.10.

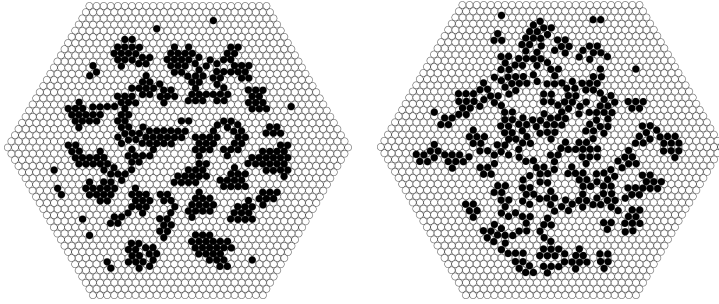


Figure 5.12: Surfaces with 400 adsorbate particles at  $\varepsilon = +1.0\%$  (left) and  $\varepsilon = +7.0\%$  (right). All other parameters are as in Fig. 5.10.

to form more, but smaller and more elongated islands. By contrast at higher values the formation of a few larger islands is preferred. An example of this effect is shown in Fig. 5.11, where two systems with  $\varepsilon = -7.0\%$  and  $\varepsilon = -1.0\%$ , respectively, are presented. Here the islands on the left surface with  $\varepsilon = -7.0\%$  are more compact and the coarsening is more advanced than on the right surface.

This effect originates from the higher diffusion barriers at step edges if the misfit is lower, which is in good agreement with the results presented in Sec. 5.2.2. The adatoms tend to remain at a step edge position and form rough island borders, at which further particles can find particularly favorable binding sites with many neighbors and high binding energies. As a consequence the islands are growing.

In the case of positive misfit, see  $\varepsilon = +5.0\%$  in the lower row of Fig. 5.10, the effect of coarsening is also evident. However, at small coverages in the beginning many single particles are diffusing on the surface and at a later time one can still find some single adatoms. In contrast to the case of negative misfit the islands do not have that compact, but rather elongated forms. These structures lead to less strain within the islands and are therefore favored. Nevertheless, all adsorbate particles merge to one large island in the end. If the misfit is positive the adatoms are not as well bound at step edges as particles with negative misfit and, thus, the process of detachment from the step edge has a larger probability for particles with positive misfit. Therefore, more single adatoms and small islands with only a few particles are visible.

The variation of misfit has, in the case of positive misfit, also a strong influence

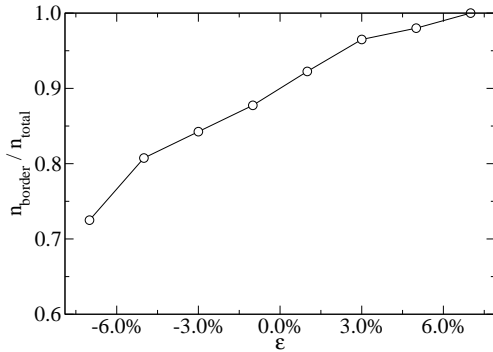


Figure 5.13: The ratio between the number of adsorbate particles at an island border and the total number of adsorbate particles vs. the misfit at the energies  $E_S = 3\text{ eV}$  and  $E_A = 0.75\text{ eV}$ .

on the emerging structures. Fig. 5.12 shows two systems with different  $\varepsilon$ . A smaller value leads to compact islands, but at higher misfits the particles can not form compact islands due to the fact that their preferred lattice is not suitable to the lattice given by the substrate. Therefore, the islands are very elongated and at some areas there are even rows of single adatoms.

Fig. 5.13 shows the ratio between the number of adsorbate particles at an island border and the total number of adsorbate particles in dependence on the misfit. The graphic confirms the optical impression: small misfits lead to more compact islands with few particles at island borders and higher misfits result in elongated structures with many border particles. In the case of high misfits the particles need much space to form large compact islands, but this fact conflicts with the lattice given by the substrate crystal. Therefore structures which are less compact are preferred.

### 5.3.2 Ternary systems

In the following we study the growth of two adsorbates on a substrate crystal and investigate how the effects which are observed in the binary systems become noticeable in that case. In this context the influence of misfit and interaction energies should play an essential role.

The panel in Fig. 5.14 shows the time evolution of a system with  $E_{AB} = 0.10\text{ eV}$  and  $\varepsilon = 1.0\%$ . The process of coarsening is quite evident: in the beginning only a few islands exist, which merge in further course of the simulation. Due to the strong interaction between particles of the same type the adatoms form islands of only one sort. This separation in regions with particles of the same type persists from the beginning of the simulation until late stages.

An important point to be considered is the dependence of the structures on the misfit and the energy values in the Lennard-Jones potential. Analog to the simulations with only one adsorbate small misfits lead to compact islands of positive misfit and larger misfits result in elongated islands, as it is illustrated in Fig. 5.15. The gaps and cracks between these islands provide less strain, because

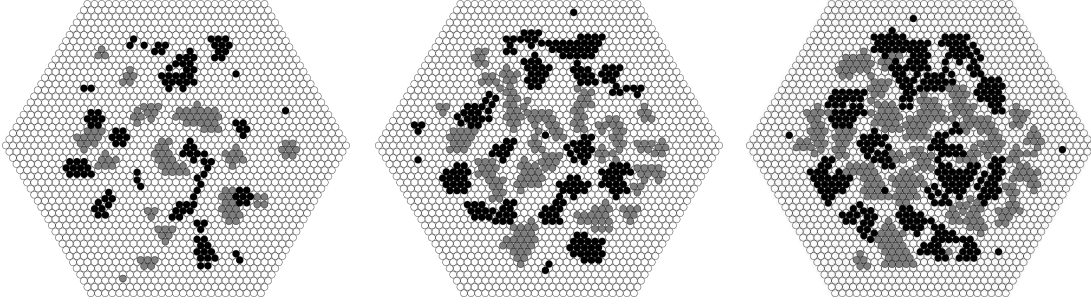


Figure 5.14: Simulation results for Lennard-Jones interactions with potential depth  $E_{AB} = 0.133 \cdot E_A = 0.10 \text{ eV}$ , and  $\varepsilon = 1.0\%$  at  $n = 250, 450, 650$  deposited adsorbate particles (from left to right). The temperature is set to  $T = 700 \text{ K}$  and the deposition rate to  $R_d = 0.0005 \text{ ML/s}$  for both types of particles. The particles with positive misfit are drawn in black.

the particles have more space to find an energetic favorable position. By contrast the regions consisting of particles with negative misfit, displayed in gray, are large at high absolute values of misfit. This behavior is in good agreement with the results with only one adsorbate (see Sec. 5.3.1). Another mechanism reducing strain is the forming of fcc and hcp islands. If two islands on different sites are located side by side a small space between the two shapes exists and the border particles can adapt their position to avoid strain within each island.

Another aspect is the influence of the interaction energy  $E_{AB}$  between the adsorbate materials. If  $E_{AB}$  is small compared to  $E_A$  and  $E_B$ , the different adsorbates have only a weak interaction with the other one resulting in a separation of the both materials. Therefore islands of only one type,  $A$  or  $B$ , are formed. The surfaces displayed in the upper row of Fig. 5.15 show that phase separation.

The lower row of the figure shows surfaces simulated with the same parameters, but with an interaction energy between the different adsorbates of  $E_{AB} = 0.8 \cdot E_A = 0.60 \text{ eV}$ . Due to the strong interaction between particles of different types the adsorbate materials tend to form elongated structures with a large interface instead of large, compact islands of only one atom sort. Furthermore there are significantly more small winding gaps at high  $E_{AB}$  than at lower energies, at which a few larger regions without any particle between the islands predominate.

However, one can observe an influence of the misfit on the island formation as well as in the case of weak interaction. The higher the value of  $E_{AB}$  the stronger is the effect of meandering. Clearly noticeable are the many single atoms with positive misfit which are surrounded by the smaller adatoms. The main reason of this behavior is the interaction energy, but an increasing misfit amplifies this effect. In the system with  $\varepsilon = 6\%$  many single particles and dimers exist which are enclosed by the adsorbate with negative misfit.

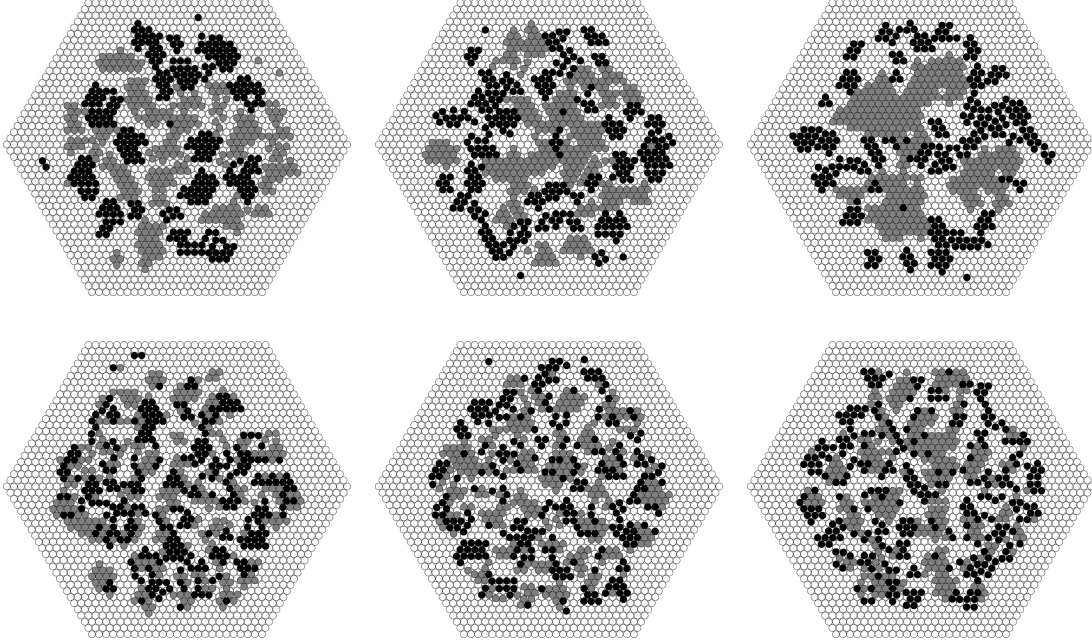


Figure 5.15: Upper row: Simulation results for Lennard-Jones interactions with  $E_{AB} = 0.133 \cdot E_A = 0.10 \text{ eV}$ , and  $\varepsilon = 1.0\%, 4.0\%, 6.0\%$  (from left to right) at  $n = 600$  deposited adsorbate particles. The temperature is set to  $T = 700 \text{ K}$  and the deposition rate to  $R_d = 0.0005 \text{ ML/s}$  for both types of particles. Lower row: Simulation results for  $E_{AB} = 0.8 \cdot E_A = 0.60 \text{ eV}$ , all other parameters as above.

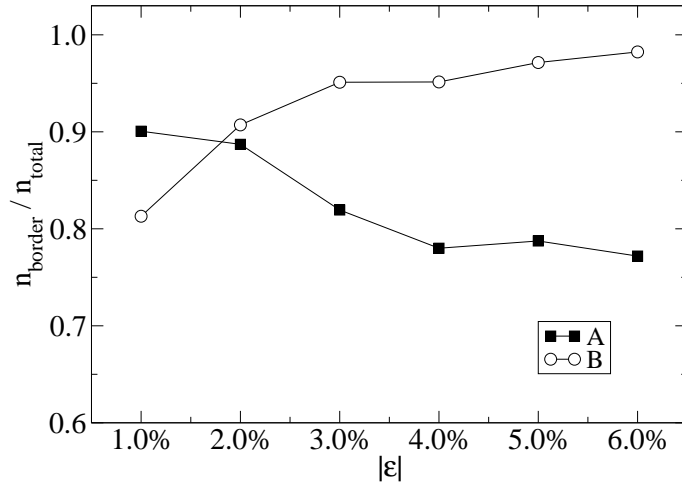


Figure 5.16: The ratio between the number of  $A$  ( $B$ ) particles at an island border and the total number of  $A$  ( $B$ ) particles vs. the absolute value of misfit  $|\varepsilon|$  at the energies  $E_S = 3 \text{ eV}$ ,  $E_A = E_B = 0.75 \text{ eV}$ ,  $E_{AB} = 0.20 \text{ eV}$  and the particle concentrations  $\eta_A = \eta_B = 0.5$ .

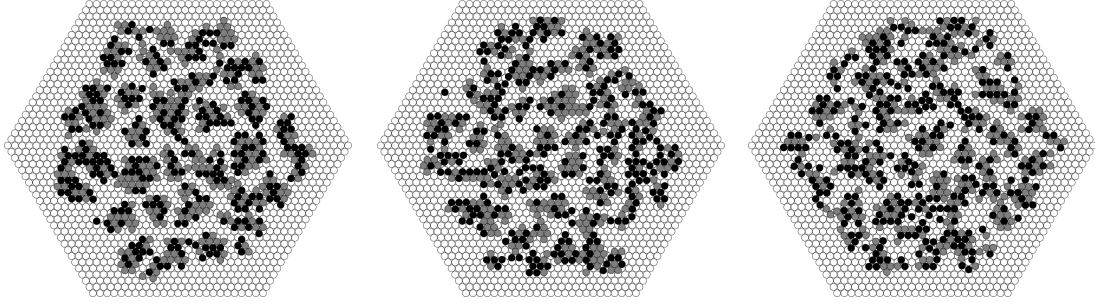


Figure 5.17: Left hand side: Simulation results for Lennard-Jones interactions with  $E_{AB} = 1.333 \cdot E_A = 1.00 \text{ eV}$ , and  $\varepsilon = 1.0\%$  at  $n = 600$  deposited adsorbate particles. The temperature is set to  $T = 700 \text{ K}$  and the deposition rate to  $R_d = 0.0005 \text{ ML/s}$  for both types of particles. Center: Results for the same energies, but  $\varepsilon = 5.0\%$ . Right hand side: Results for  $E_{AB} = 2 \cdot E_A = 1.50 \text{ eV}$ , and  $\varepsilon = 1.0\%$ .

Analog to the results in the case of only one adsorbate material, the part of border particles depends on the misfit. The measurement of the ratio between the number of  $A$  ( $B$ ) particles at an  $A$  ( $B$ ) island border and the total number of  $A$  ( $B$ ) particles in dependence on the misfit leads to a curve displayed in Fig. 5.16. At low misfits the part of the larger  $B$  atoms, which are at a border, is rather low, but increases with increasing misfit. On the other hand, the smaller  $A$  particles show a contrary behavior in the graphic. Due to the fact that their misfit decreases with increasing absolute value, the part of border particles of them decreases. Hence the adatoms in a system with two sorts of adsorbates form islands in a very similar manner like in systems with only one type of adsorbate. However, the interaction of the different adsorbates influences this effect pretty strongly.

If the interaction between particles of different type is stronger than between adatoms of the same type,  $E_{AB} > E_A, E_B$ , the situation changes and different structures are emerging. Three examples of such a configuration at two different misfits and energies are shown in Fig. 5.17. In all three cases many small islands consisting of different adsorbates are formed. The islands have no compact shapes and are rather craggy.

Due to the strong interaction between the two different adsorbate sorts  $A$  and  $B$  every particle aspires to a position at which it has so many particles of the other type in his neighborhood as possible. One consequence is that hardly any adatoms have six neighbor particles of their own sort and hence no large islands of only one sort are built. Instead, short stripes of one adsorbate are formed in many islands. Particularly the rows of black particles, which are surrounded by smaller gray particles, are evident.

The effect of interaction is very strong and as a result the misfit has no

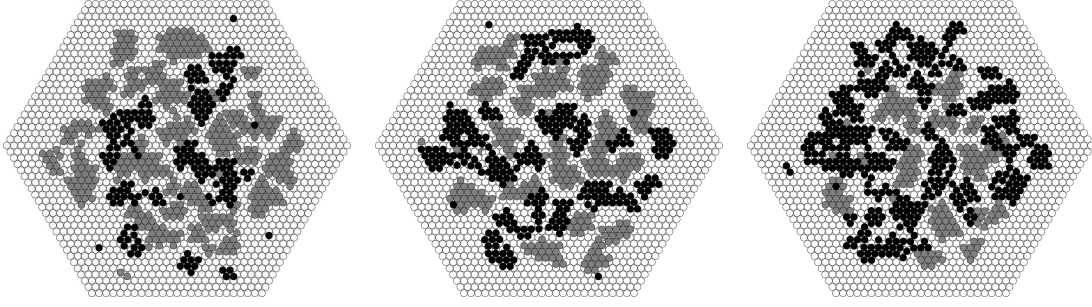


Figure 5.18: Simulation results for Lennard-Jones interactions with  $E_{AB} = 0.2666 \cdot E_A = 0.20 \text{ eV}$ , and  $\varepsilon = 2.0\%$  at  $n = 600$  deposited adsorbate particles. The concentrations are  $\eta_A = 0.7, 0.5, 0.3$  (from left to right) and the temperature is set to  $T = 700 \text{ K}$  and the deposition rate to  $R_d = 0.0005 \text{ ML/s}$  for both types of particles.

evident influence. Furthermore there is no appreciable difference between systems with various energies  $E_{AB,1} \neq E_{AB,2}$  if both energies are higher than  $E_A$  and  $E_B$ . Already systems with energies  $E_{AB}$  curtly above  $E_{A,B}$  show this behavior independent of the lattice mismatch. However, at lower energies the particles with the negative misfit tend to build sometimes a little bit thicker stripes. By contrast, at high energies the stripes have a thickness of only one particle. But this effect is very small and, thus, the structures in all pictures in Fig. 5.17 are very similar.

Up to now we considered only surfaces with approximately as many  $A$  particles as  $B$  particles. But it is an interesting point what happens at different concentrations of adsorbates. To investigate according configurations we deposit  $A$  and  $B$  particles with probabilities  $p_{d,A}$  and  $p_{d,B}$ , respectively. The resulting adsorbate consists of the two types corresponding to the concentrations  $\eta_A$  and  $\eta_B$  with  $\eta_A + \eta_B = 1$ .

Fig. 5.18 shows some simulation results of different adsorbate concentrations in the case of  $E_{AB} < E_A = E_B$ . At  $\eta_A = 0.7$  and  $\eta_B = 0.3$  (left picture) a few small islands of  $B$  particles and some large, compact islands consisting of  $A$  particles around them are grown. In the next graphic a surface with  $\eta_A = \eta_B = 0.5$  is pictured. Here, the structures have the already described characteristics depending on the energies and the misfit. Note that there are approximately the same number of islands of each adsorbate sort. The last picture on the right hand side shows a system with  $\eta_A = 0.3$  and  $\eta_B = 0.7$ . The smaller adatoms form compact islands in contrast to the  $B$  particles, which prefer a meandering structure due to their positive misfit. In all three cases the smaller  $A$  particles build compact islands similar to the structures in binary systems. By contrast the  $B$  particles tend to elongated islands avoiding strain. These results are in good agreement with the previous results of ternary systems at  $\eta_A = \eta_B = 0.5$



and binary systems at  $\eta_A = 1$  or  $\eta_B = 1$ , respectively.

## 5.4 Comparison with equilibrium simulations

We have investigated the influence of different parameters on the form of structures both in equilibrium and growth simulations. In both cases large islands of positive misfit are formed for small misfits and interaction energies  $E_{AB} < E_A, E_B$ . In equilibrium simulations, the smaller particles of negative misfit are arranged around these islands and on the grown surfaces the smaller particles also tend to this behavior. In both types of simulations the influence of the energy is strong, but at growth the energy effect dominates the formation of adsorbate structures. Nevertheless, an influence of the misfit can definitely be observed.

With increasing  $E_{AB}$  the number of islands increases and their average size decreases in equilibrium simulations. By contrast, the variation of these parameters in the growth model results in a change of the island form with more elongated shapes. But in both cases the part of border particles increases and more particles of different sorts are side by side. Due to the energy value this configuration is preferred.

A very similar effect can be observed if the lattice mismatch is varied. At larger misfits the system has to reduce the emerging strain. This reducing of strain can be realized by forming smaller islands (equilibrium) as well as elongated islands (growth). In both scenarios the part of border particles increases. However, in the case of growth the particles can switch from an fcc to a hcp site and vice versa. The small space, which results from this step, leads to a reduction of strain and enables the formation of large, but elongated islands also at higher misfits.

If the interaction between particles of different type is higher than that of the same sort in equilibrium simulations,  $E_{AB} > E_A, E_B$ , the adsorbates form stripes, whose number of bendings depends on the misfit. This effect results in a large interface and is energetically favored. In growth simulations there are no large islands of only one adsorbate type, but rather mixed islands consisting of short stripes of one adsorbate and a couple of single particles surrounded by adatoms of the other type. However, the misfit has almost no influence in this case.

If the concentration of both adsorbates  $A$  and  $B$  is varied, the previously described formation of islands is disordered at certain configurations. In equilibrium large islands of  $B$  particles are formed at high  $\eta_B$ , but at low values the average island size depends only weakly on the concentration. The behavior at growth is analog: at small  $\eta_B$  small compact islands of  $B$  particles are embedded in one large island of the smaller particles of adsorbate  $A$ . The size of  $B$  islands is rather constant for small variations of the concentrations within this range. If the value of  $\eta_B$  is high, large islands of  $B$  particles, which surround the  $A$  islands, exist, but the shapes are elongated reducing the strain within the islands. The

smaller adatoms of type  $A$  in contrast form always compact islands.

In summary, one can say that the equilibrium and the growth simulations have a great deal in common. There exist many similarities, but there are also some minor differences by nature.

## 5.5 Conclusions

In this chapter we have studied epitaxial growth on an fcc substrate crystal by means of Kinetic Monte Carlo simulations and the influence of different parameters on the emerging structures. To keep the computational effort within a feasible limit we have used a ball and spring like model.

At first we have investigated energies and diffusion barriers which play an important role at growth. On plane surfaces both the binding energy and the transition energy decrease with increasing misfit, and in the same way the diffusion barrier diminishes. Here, the adatoms show the same behavior on fcc as well as on hcp sites and the particles have on both sites almost the same energy value. Indeed, at step edges the binding energy looks a little bit more complicated, but the activation energy of a diffusion step decreases too.

On inspection of systems with only one adsorbate component it was shown that small misfits lead to compact islands, while at large positive values of  $\varepsilon$  elongated structures with many border particles are preferred. These island shapes reduce strain and are favorable in respect of energy. At negative misfits the particles have enough space to arrange side by side and are well bound by the neighboring adsorbate particles. Therefore they form large compact islands. Due to the fact that there exists almost no difference between the binding energies on fcc and hcp sites, both fcc and hcp islands emerge.

As expected ternary systems show a very similar behavior to the binary systems in terms of compactness. The energy  $E_{AB}$  has a very strong influence on the structure evolution. Small values  $E_{AB} < E_A, E_B$  result in separation of both components with islands of only one adsorbate sort in contrast to higher energies which cause mixed islands. Simultaneously, a high absolute value of the lattice mismatch  $|\varepsilon|$  leads to a reduction of the compactness of the  $B$  islands and, hence, lowers the adsorbate separation. If the interaction energy of heterogeneous adatoms exceeds the interaction between two particles of the same type,  $E_{AB} > E_A, E_B$ , mixed islands consisting of particles of both adsorbates are emerging. Small rows of particles of one sort and single particles frequently appear in this configuration. A variation of the adsorbate concentrations leads to expectable results similar to binary systems. At small  $\eta_B$  the average size of  $B$  islands is quite constant.

Altogether, the results of the growth simulations are in good agreement to those of the equilibrium simulations in chapter 4. In both cases the interaction energy  $E_{AB}$  and the misfit play an essential role in the formation of struc-

tures. Large values of both interaction energy and misfit tend to smaller or more elongated islands of  $B$  particles in contrast to smaller values, which result in a separation of the two adsorbates.



# Chapter 6

## Conclusions and outlook

In this thesis, simulations of fcc crystals grown by molecular beam epitaxy has been studied. Today, computer simulations are a very powerful tool for the design of novel technical applications. The aim of this work has been the investigation of the pattern formation on a flat surface, if two adsorbate materials with different lattice constants are deposited. The results can give important information about the influence of the different single parameters on the emerging structures. The knowledge of such facts can help to understand which procedures are of significance at the production of high quality crystals.

In our simulations we have used an off-lattice model, which allows the investigation of crystals consisting of materials with different lattice constants. The goal has been the investigation of the emerging structures in the first monolayer upon a [111] substrate. In order to simulate the interaction between the particles we have used a simple pair potential: the Lennard-Jones potential. Due to the high computational costs of off-lattice simulations some simplifications has been necessary in order to realize the study of crystals at a certain size.

In the case of equilibrium simulations, the interplay between misfit and interaction energy results in different structures. By variation of  $\varepsilon$  and  $E_{AB}$  configurations like the complete separation of the adsorbates or different forms and sizes of islands are realizable. If the interaction energy between different adsorbates is larger than that between same species,  $E_{AB} > E_A, E_B$ , stripe-like structures are formed. Other parameters which have a large influence on the grown structures are the adsorbate concentrations, whereas the temperature plays only a secondary role in this context. A convenient choice of adsorbate concentrations and interaction energies results in the formation of 2D droplets.

To keep the simulation times of the growth simulations within a feasible limit, we have used a ball and spring like model with precalculated transition energies depending on the number of neighboring particles. Further on, we use continuous coordinates in order to take the lattice mismatch into account. This approach allows determining energy barriers in a fast way and permits the simulation of growth at interesting crystal sizes and temperatures. With the misfit and the

interaction energy between two different adsorbate materials the island forms can be controlled and the emerging structures show a similar behavior to analog systems in the equilibrium simulations.

We observe qualitatively the same dependence on misfit and interaction energy both in the case of equilibrium simulations and in the case of growth simulations. Both approaches leads to very similar results and show how some parameters influence the epitaxial growth of crystals, whereas the impact of other variables is rather of small importance. Thus, we have been able to show that parameters like the interaction energy, the misfit and the particle concentrations are the determining factors in our model of molecular beam epitaxy with two different adsorbates, naturally in consideration of the fact that many simplifications have been necessary to realize off-lattice Monte Carlo simulations.

Further investigations should aim at larger system sizes, since some structures need more space to develop and to become evident. However, that large systems are hardly realizable actually, but in the future better computer power should help to tackle this problem.

Another point to be considered could be the implementation of more processes like, e.g., the exchange diffusion. However, in this context it is necessary to look after the considered components. Different material combinations can even cause different processes. Thus, it is possible to adapt the simulation to specific materials and to get results which are closer to real structures. In this context more realistic and more sophisticated potentials are of particular interest. The difficulty in the use of such potentials are the enormous costs in simulation time, which limit the actual feasibility.

In the face to technical applications the simulation of multi-layer systems plays a very important role. Therefore it would be very promising to expand our simulations, which have been limited to one monolayer, to a few layers. Then further important aspects of crystal growth like, e.g., the generation of dislocations in three dimensions can be explored. The simulation of other crystal structures and surfaces will require further modifications of the models.

The used method of Monte Carlo simulations provides important insights at the study of epitaxial growth and bridges the gap between Molecular Dynamics simulations and lattice-gas models. Therefore, that approach should also play an essential role in future investigations in the field of condensed matter and material science.

# Appendix A

## Lennard-Jones potential

In computer simulations of metals simple pair potentials are widely used although the interatomic forces are not simple. One of the most used potentials in this context is the Lennard-Jones potential consisting of two parts: an attractive one at long distances and a repulsive one at short distances. If the distance of two interacting particles is large, the attractive forces preponderate, but in a certain distance the repulsive part begins strongly to increase, representing the Pauli repulsion. Due to its simplicity the Lennard-Jones potential is often used to describe the interactions of gases or neutral atoms, but it yields also a rough approximation for metals.

In many cases the Lennard-Jones 12,6 potential [58, 86, 87]

$$U(r_{ij}) = 4 E_{ij} \left[ \left( \frac{\sigma_{ij}}{r_{ij}} \right)^{12} - \left( \frac{\sigma_{ij}}{r_{ij}} \right)^6 \right] \quad (\text{A.1})$$

is used. Here,  $r_{ij}$  is the distance between the two particles  $i$  and  $j$ ,  $-E_{ij}$  the depth of the potential and  $\sigma_{ij}$  the distance at which the interparticle force is zero.

The attractive long-range part  $\propto r_{ij}^{-6}$  represents the Van der Waals attractions in inert gas crystals, but the repulsive term  $\propto r_{ij}^{-12}$  is not motivated by physical reasons. However, it is very convenient due to the efficient computing of  $r^{-12}$  as a square of  $r^{-6}$ .

A more generalized form of the Lennard-Jones n,m potential [87] is given by

$$U(r_{ij}) = E_{ij} \left[ \frac{m}{n-m} \left( \frac{r_{ij}^0}{r_{ij}} \right)^n - \frac{n}{n-m} \left( \frac{r_{ij}^0}{r_{ij}} \right)^m \right] \quad (n > m) \quad (\text{A.2})$$

with the equilibrium distance  $r_{ij}^0$  between the particles and their dissociation energy  $E_{ij}$ . Two further parameters are  $n$  and  $m$ . The adaption of these four parameters based on experimental data yields more realistic results.

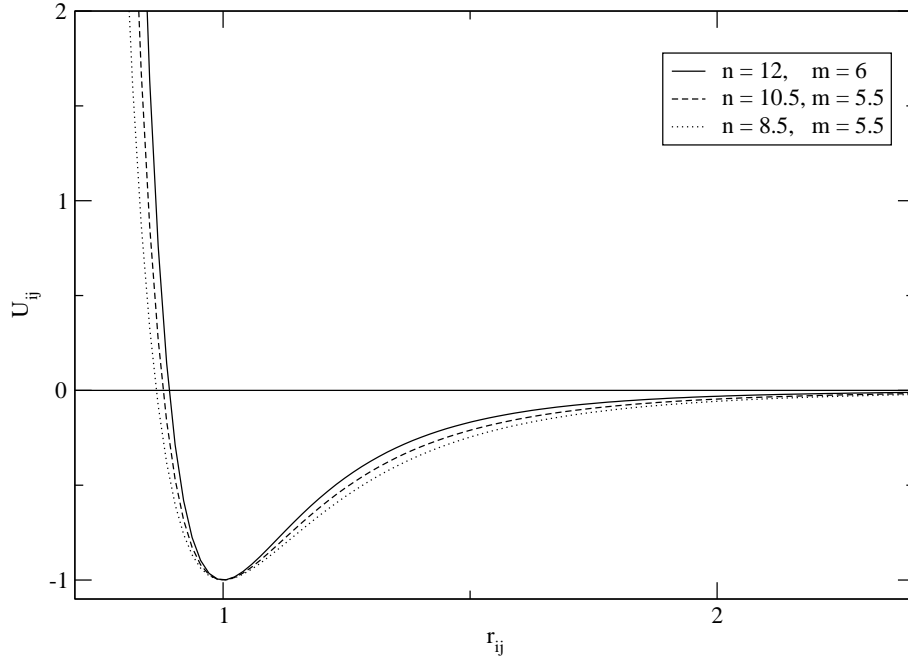


Figure A.1: Lennard-Jones  $n, m$  potentials for  $E_{ij} = 1$  and  $r_{ij}^0 = 1$ .

The equilibrium distance is proportional to  $\sigma_{ij}$  and for the case  $n = 2m$  the minimum is reached at the distance

$$r_{ij}^0 = \sqrt[n-m]{\frac{n}{m}} \sigma_{ij}. \quad (\text{A.3})$$

Fig. A.1 shows Lennard-Jones potentials for different values of  $n$  and  $m$ . The parameters  $n$  and  $m$  affect the form of the graph around the equilibrium distance, but for large distances the differences decrease and the potentials converge to  $U(r_{ij}) = 0$  for  $r_{ij} \rightarrow +\infty$ .



# Appendix B

## Equilibrium distances

The equilibrium distances of the atoms in a lattice depend on the number of neighbors and their distances [58, 109]. In the case of the fcc structure every atom has 12 nearest neighbors in a distance  $a/\sqrt{2}$  with the length of the unit cell  $a$  and in distance  $a$  there are 6 particles and so on (see Sec. 3). We look at a particle and write the distance to another particle  $j$  as  $R_j = r_j R$  so that  $r_j$  is the distance in units of  $a/\sqrt{2}$ , the distance between nearest neighbors. Thus, the summation over all interactions in the Lennard-Jones 12,6 potential yields

$$\sum_j \frac{1}{R_j^6} = \frac{1}{R^6} \sum_j \frac{1}{r_j^6} = \frac{1}{R^6} \left( 12 \frac{1}{1} + 6 \frac{1}{8} + 12 \frac{1}{64} + \dots \right) = \frac{1}{R^6} 14.45 \quad (\text{B.1})$$

and

$$\sum_j \frac{1}{R_j^{12}} = \frac{1}{R^{12}} \sum_j \frac{1}{r_j^{12}} = \frac{1}{R^{12}} \left( 12 \frac{1}{1} + 6 \frac{1}{64} + \dots \right) = \frac{1}{R^{12}} 12.13. \quad (\text{B.2})$$

Hence the interaction energy results in

$$U(R) = \frac{1}{2} \sum_{ij} U_{ij}(R_{ij}) = 2N\varepsilon \left[ 12.13 \left( \frac{\sigma}{R} \right)^{12} - 14.45 \left( \frac{\sigma}{R} \right)^6 \right] \quad (\text{B.3})$$

with the number of atoms  $N$  in the system. The equilibrium distance  $R_0$  is calculated by minimization of the energy:

$$\left. \frac{dU}{dR} \right|_{R_0} = -2N\varepsilon \left[ 12 \cdot 12.13 \frac{\sigma^{12}}{R_0^{13}} - 6 \cdot 14.45 \frac{\sigma^6}{R_0^7} \right] = 0 \quad (\text{B.4})$$

$$145.56 \sigma^6 = 86.7 R_0^6 \quad (\text{B.5})$$

This leads to the equilibrium distance  $R_0 \approx 1.09 \sigma$ .



# Appendix C

## Evolution into equilibrium

An interesting point with regard to the results of our simulations is the question how many MC steps are needed until the systems are in equilibrium. For that purpose we have a look at the surfaces after different numbers of steps. Fig. C.1 shows an example of such an evolution of a system with  $E_{AS} = 0.45 eV$  and  $\varepsilon = 4.5\%$  during the equilibrium simulation. In the beginning, the adsorbate particles are randomly arranged, but at this parameter set the equilibrium is reached very fast and after that there are only a few small changes in the surface structures.

The optical impression is proved by the plots in Fig. C.2. Already after a few thousand steps, the average island size as well as the number of islands are both quite constant and the graphics show only a few fluctuations. In the case of  $E_{AS} = 0.35 eV$  and  $\varepsilon = 5.5\%$ , which is displayed in Fig. C.3, the systems need more steps to attain the equilibrium, but after  $100 \cdot 10^3$  steps the number of islands and their average size is constant with almost no fluctuations due to the

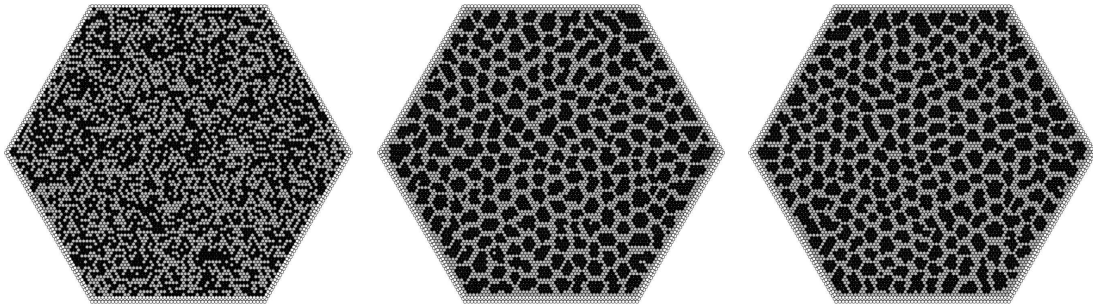


Figure C.1: Simulation results for Lennard-Jones interactions with  $E_S = 3.00 eV$ ,  $E_A = 0.50 eV$ ,  $E_{AS} = 0.45 eV$ , and  $\varepsilon = 4.5\%$ : initial configuration and the configurations after  $60 \cdot 10^3$  and after  $140 \cdot 10^3$  MC steps (from left to right). The temperature is set to  $T = 250 K$ . The particles with positive misfit are drawn in black.

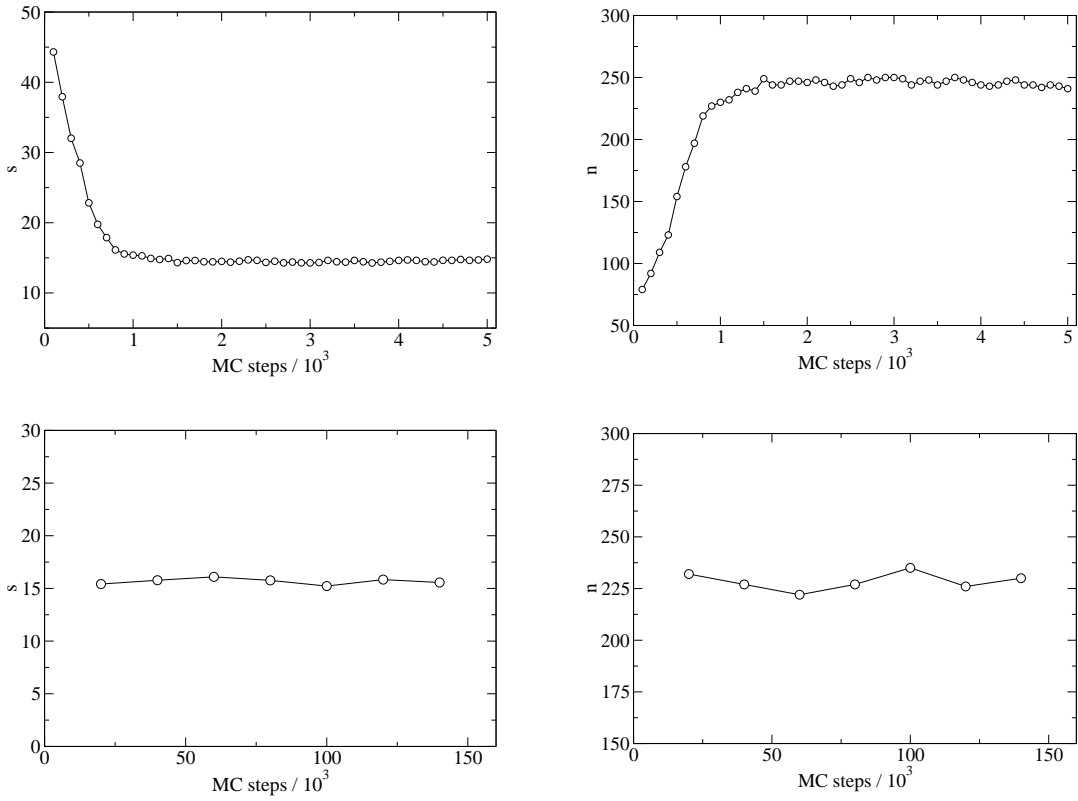


Figure C.2: Left: The average island size  $s$  consisting of  $B$  particles vs. the number of MC steps at  $E_{AB} = 0.45 \text{ eV}$  and  $\varepsilon = 4.5\%$ . Right: The number of  $B$  islands  $n$  vs. the number of MC steps at the same parameters.

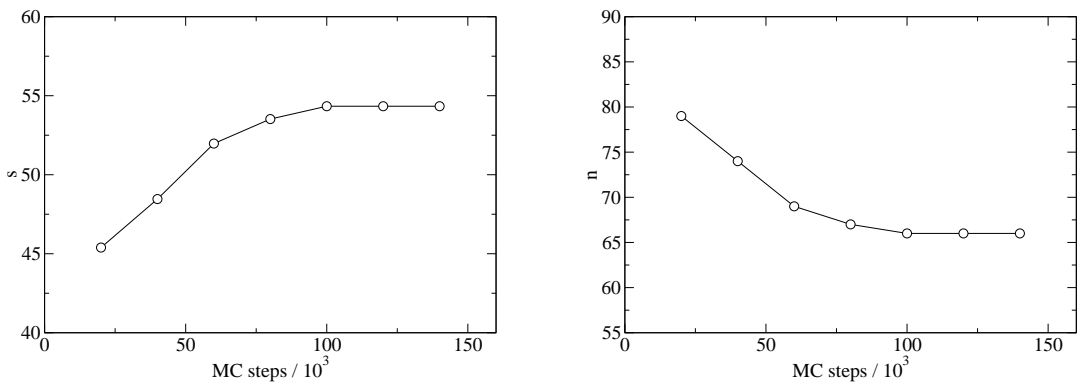


Figure C.3: Left: The average island size  $s$  consisting of  $B$  particles vs. the number of MC steps at  $E_{AB} = 0.35 \text{ eV}$  and  $\varepsilon = 5.5\%$ . Right: The number of  $B$  islands  $n$  vs. the number of MC steps at the same parameters.

large island sizes. At the beginning of the simulation, many steps are necessary in order to form the large islands appropriate to this set of parameters.

The smaller the islands the stronger are the influences of the fluctuations on the structures since smaller islands can completely decay by small fluctuations. Thus, the number of islands strongly fluctuates if the average island size is very small.

In almost all our simulations the equilibrium is reached after  $10^5$  steps at the latest and the simulation can be stopped. However, in the most cases the equilibrium is reached even earlier.



# Bibliography

- [1] A. Zangwill. *Physics at Surfaces*. Cambridge University Press, Cambridge, 1988.
- [2] C. B. Duke, editor. *Surf. Sci.: The First Thirty Years*. North-Holland, Amsterdam, 1994. Reprinted from *Surf. Sci.*, 299/300, 1994.
- [3] M. A. Herman and H. Sitter. *Molecular Beam Epitaxy - Fundamentals and Current Status*. Springer, Berlin, 2nd edition, 1996.
- [4] P. Politi, G. Grenet, A. Marty, A. Ponchet, and J. Villain. Instabilities in crystal growth by atomic or molecular beams. *Physics Reports*, 324(5-6):271–404, 2000.
- [5] E. H. C. Parker, editor. *The Technology and Physics of Molecular Beam Epitaxy*. Plenum Press, New York, 1985.
- [6] A. Pimpinelli and J. Villain. *Physics of Crystal Growth*. Cambridge University Press, Cambridge, 1998.
- [7] A.-L. Barabási and H. E. Stanley. *Fractal Concepts in Surface Growth*. Cambridge University Press, Cambridge, 1995.
- [8] J. W. Evans, D. E. Sanders, P. A. Thiel, and A. E. DePristo. Low-temperature epitaxial growth of thin metal films. *Phys. Rev. B*, 41(8):5410–5413, 1990.
- [9] J. D. Wrigley and G. Ehrlich. Surface Diffusion by an Atomic Exchange Mechanism. *Phys. Rev. Lett.*, 44(10):661–663, 1980.
- [10] F. Máca, M. Kotrla, and O. S. Trushin. Energy barriers for diffusion on stepped Pt(111) surface. *Vacuum*, 54(1-4):113–117, 1999.
- [11] F. Máca, M. Kotrla, and O. S. Trushin. Energy barriers for diffusion on stepped Rh(111) surfaces. *Surf. Sci.*, 454-456:579–583, 2000.
- [12] C.-L. Liu and J. B. Adams. Diffusion behavior of single adatoms near and at steps during growth of metallic thin films on Ni surfaces. *Surf. Sci.*, 294(3):197–210, 1993.

- 
- [13] R. Q. Hwang. Chemically Induced Step Edge Diffusion Barriers: Dendritic Growth in 2D Alloys. *Phys. Rev. Lett.*, 76(25):4757–4760, 1996.
- [14] T. Volkmann, F. Much, M. Biehl, and M. Kotrla. Interplay of strain relaxation and chemically induced diffusion barriers: Nanostructure formation in 2D alloys. *Surf. Sci.*, 586(1-3):157–173, 2005.
- [15] E. D. Tober, R. F. C. Farrow, R. F. Marks, G. Witte, K. Kalki, and D. D. Chambliss. Self-Assembled Lateral Multilayers from Thin Film Alloys of Immiscible Metals. *Phys. Rev. Lett.*, 81(9):1897–1900, 1998.
- [16] R. Q. Hwang and M. C. Bartelt. Scanning Tunneling Microscopy Studies of Metal on Metal Epitaxy. *Chem. Rev.*, 97:1063–1082, 1997.
- [17] G. E. Thayer, V. Ozolins, A. K. Schmid, N. C. Bartelt, M. Asta, J. J. Hoyt, S. Chiang, and R. Q. Hwang. Role of Stress in Thin Film Alloy Thermodynamics: Competition between Alloying and Dislocation Formation. *Phys. Rev. Lett.*, 86(4):660–663, 2001.
- [18] J. L. Stevens and R. Q. Hwang. Strain Stabilized Alloying of Immiscible Metals in Thin Films. *Phys. Rev. Lett.*, 74(11):2078–2081, 1995.
- [19] B. Sadigh, M. Asta, V. Ozoliņš, A. K. Schmid, N. C. Bartelt, A. A. Quong, and R. Q. Hwang. Short-Range Order and Phase Stability of Surface Alloys: PdAu on Ru(0001). *Phys. Rev. Lett.*, 83(7):1379–1382, 1999.
- [20] A. K. Schmid, J. C. Hamilton, N. C. Bartelt, and R. Q. Hwang. Surface Alloy Formation by Interdiffusion across a Linear Interface. *Phys. Rev. Lett.*, 77(14):2977–2980, 1996.
- [21] M. Kotrla. Numerical simulations in the theory of crystal growth. *Comput. Phys. Commun.*, 97:82–100, 1996.
- [22] T. Michely and J. Krug. *Islands, Mounds and Atoms - Patterns and Processes in Crystal Growth Far from Equilibrium*. Springer, Berlin, 2004.
- [23] M. Biehl. Lattice gas models and kinetic monte carlo simulations of epitaxial growth. In A. Voigt, editor, *Multiscale Modeling in Epitaxial Growth, International Series of Numerical Mathematics*, volume 149, pages 3–18. Birkhäuser, 2005.
- [24] M. Biehl, F. Much, and C. Vey. Off-lattice kinetic monte carlo simulations of strained heteroepitaxial growth. In A. Voigt, editor, *Multiscale Modeling in Epitaxial Growth, International Series of Numerical Mathematics*, volume 149, pages 41–57. Birkhäuser, 2005.



- [25] W. Kohn and L. J. Sham. Self-Consistent Equations Including Exchange and Correlation Effects. *Phys. Rev.*, 140(4A):A1133–A1138, 1965.
- [26] P. Hohenberg and W. Kohn. Inhomogeneous Electron Gas. *Phys. Rev.*, 136(3B):B864–B871, 1964.
- [27] R. M. Dreizler and E. K. U. Gross. *Density Functional Theory - An Approach to the Quantum Many-Body Problem*. Springer, Berlin, 1990.
- [28] E. K. U. Gross and R. M. Dreizler. *Density Functional Theory*. Plenum Press, New York, 1995.
- [29] F. Jensen. *Introduction to Computational Chemistry*. Wiley, Chichester, 1999.
- [30] C. H. Park and D. J. Chadi. First-principles study of the atomic reconstructions of ZnSe(100) surfaces. *Phys. Rev. B*, 49(23):16467–16473, 1994.
- [31] S. Gundel, A. Fleszar, W. Faschinger, and W. Hanke. Atomic and electronic structure of the CdTe(001) surface: LDA and GW calculations. *Phys. Rev. B*, 59(23):15261–15269, 1999.
- [32] G. Brocks, P. J. Kelly, and R. Car. Binding and diffusion of a Si adatom on the Si(100) surface. *Phys. Rev. Lett.*, 66(13):1729–1732, 1991.
- [33] C. Ratsch and M. Scheffler. Density-functional theory calculations of hopping rates of surface diffusion. *Phys. Rev. B*, 58(19):13163–13166, 1998.
- [34] L. Weinhardt, O. Fuchs, E. Umbach, C. Heske, A. Fleszar, W. Hanke, and J. D. Denlinger. Resonant inelastic soft x-ray scattering, x-ray absorption spectroscopy, and density functional theory calculations of the electronic bulk band structure of CdS. *Phys. Rev. B*, 75:165207, 2007.
- [35] B. J. Alder and T. E. Wainwright. Phase Transition for a Hard Sphere System. *J. Chem. Phys.*, 27(5):1208–1209, 1957.
- [36] B. J. Alder and T. E. Wainwright. Studies in Molecular Dynamics. I. General Method. *J. Chem. Phys.*, 31(2):459–466, 1959.
- [37] J. M. Haile. *Molecular Dynamics Simulation - Elementary Methods*. Wiley, New York, 1992.
- [38] R. Haberland, S. Fritzsche, G. Peinel, and K. Heinzinger. *Molekularodynamik - Grundlagen und Anwendungen*. Vieweg, Braunschweig, 1995.
- [39] R. Car and M. Parrinello. Unified Approach for Molecular Dynamics and Density-Functional Theory. *Phys. Rev. Lett.*, 55(22):2471–2474, 1985.

- 
- [40] Godehard Sutmann. Classical molecular dynamics. In J. Grotendorst, D. Marx, and A. Muramatsu, editors, *Quantum Simulations of Complex Many-Body Systems: From Theory to Algorithms, Lecture Notes*, volume 10, pages 211–254. John von Neumann Institute for Computing, Jülich, NIC Series, 2002.
- [41] C. M. Gilmore and J. A. Sprague. Molecular-dynamics simulation of the energetic deposition of Ag thin films. *Phys. Rev. B*, 44(16):8950–8957, 1991.
- [42] E. Aubin and L. J. Lewis. Growth of metallic superlattices by sequential deposition of atoms. *Phys. Rev. B*, 47(11):6780–6783, 1993.
- [43] M. F. Crowley, D. Srivastava, and B. J. Garrison. Molecular dynamics investigation of the MBE growth of Si on Si110. *Surf. Sci.*, 284:91–102, 1993.
- [44] O. S. Trushin, M. Kotrla, and F. Máca. Energy barriers on stepped Ir/Ir(111) surfaces: a molecular statics calculation. *Surf. Sci.*, 389:55–65, 1997.
- [45] N. Metropolis, A. W. Rosenbluth, M. N. Rosenbluth, A. H. Teller, and E. Teller. Equation of State Calculations by Fast Computing Machines. *J. Chem. Phys.*, 21(6):1087–1092, 1953.
- [46] M. E. J. Newman and G. T. Barkema. *Monte Carlo Methods in Statistical Physics*. Clarendon Press, Oxford, 1999.
- [47] D. P. Landau and K. Binder. *A Guide to Monte Carlo Simulations in Statistical Physics*. Cambridge University Press, Cambridge, 2000.
- [48] W. Kinzel and G. Reents. *Physik per Computer*. Spektrum, Heidelberg, 1996.
- [49] G. Russo, L. M. Sander, and P. Smereka. Quasicontinuum Monte Carlo: A method for surface growth simulations. *Phys. Rev. B*, 69:121406, 2004.
- [50] T. P. Schulze and W. E. A continuum model for the growth of epitaxial films. *J. Cryst. Growth*, 222(1-2):414–425, 2001.
- [51] S. F. Edwards and D. R. Wilkinson. The Surface Statistics of a Granular Aggregate. *Proc. R. Soc. London A*, 381:17–31, 1982.
- [52] M. Kardar, G. Parisi, and Y.-C. Zhang. Dynamic Scaling of Growing Interfaces. *Phys. Rev. Lett.*, 56(9):889–892, 1986.
- [53] E. Medina, T. Hwa, M. Kardar, and Y.-C. Zhang. Burgers equation with correlated noise: Renormalization-group analysis and applications to directed polymers and interface growth. *Phys. Rev. A*, 39(6):3053–3075, 1989.

- [54] J. Kew, M. R. Wilby, and D. D. Vvedensky. Continuous-space Monte Carlo simulations of epitaxial growth. *J. Cryst. Growth*, 127(1-4):508–512, 1993.
- [55] T. Volkman. *Lattice Gas Models and Simulations of Epitaxial Growth*. PhD thesis, Bayerische Julius-Maximilians-Universität Würzburg, Würzburg, 2004.
- [56] F. Much. *Modeling and Simulation of Strained Heteroepitaxial Growth*. PhD thesis, Bayerische Julius-Maximilians-Universität Würzburg, Würzburg, 2003.
- [57] M. Walther, M. Biehl, and W. Kinzel. Formation and consequences of misfit dislocations in heteroepitaxial growth. *Phys. Stat. Sol. (c)*, 4(9):3210–3220, 2007.
- [58] N. W. Ashcroft and N. D. Mermin. *Festkörperphysik*. Oldenbourg, München, 2001.
- [59] F. Bechstedt. *Principles of Surface Physics*. Springer, Berlin, 2003.
- [60] K. Oura, V. G. Lifshits, A. A. Saranin, A. V. Zotov, and M. Katayama. *Surface Science - An Introduction*. Springer, Berlin, 2003.
- [61] A. Schindler. *Theoretical aspects of growth on one and two dimensional strained crystal surfaces*. PhD thesis, Gerhard-Mercator-Universität Duisburg, Duisburg, 1999.
- [62] H. Spjut and D. A. Faux. Computer simulation of strain-induced diffusion enhancement of Si adatoms on the Si(001) surface. *Surf. Sci.*, 306(1-2):233–239, 1994.
- [63] G. T. Barkema and N. Mousseau. Event-Based Relaxation of Continuous Disordered Systems. *Phys. Rev. Lett.*, 77(21):4358–4361, 1996.
- [64] N. Mousseau and G. T. Barkema. Traveling through potential energy landscapes of disordered materials: The activation-relaxation technique. *Phys. Rev. E*, 57(2):2419–2424, 1998.
- [65] R. Malek and N. Mousseau. Dynamics of Lennard-Jones clusters: A characterization of the activation-relaxation technique. *Phys. Rev. E*, 62(6):7723–7728, 2000.
- [66] M. Schroeder and D. E. Wolf. Diffusion on strained surfaces. *Surf. Sci.*, 375(1):129–140, 1997.
- [67] B. G. Orr, D. Kessler, C. W. Snyder, and L. Sander. A Model for Strain-Induced Roughening and Coherent Island Growth. *Europhys. Lett.*, 19(1):33–38, 1992.

- 
- [68] A.-L. Barabási. Self-assembled island formation in heteroepitaxial growth. *Appl. Phys. Lett.*, 70(19):2565–2567, 1997.
- [69] K. E. Khor and S. Das Sarma. Quantum dot self-assembly in growth of strained-layer thin films: A kinetic Monte Carlo study. *Phys. Rev. B*, 62(24):16657–16664, 2000.
- [70] C.-H. Lam, C.-K. Lee, and L. M. Sander. Competing Roughening Mechanisms in Strained Heteroepitaxy: A Fast Kinetic Monte Carlo Study. *Phys. Rev. Lett.*, 89(21):216102, 2002.
- [71] G. Russo and P. Smereka. Computation of strained epitaxial growth in three dimensions by kinetic Monte Carlo. *J. Comput. Phys.*, 214(2):809–828, 2006.
- [72] W. H. Press, S. A. Teukolsky, W. T. Vetterling, and B. P. Flannery. *Numerical Recipes in C*. Cambridge University Press, Cambridge, second edition, 1992.
- [73] A. B. Bortz, M. H. Kalos, and J. L. Lebowitz. A new algorithm for Monte Carlo simulation of Ising spin systems. *J. Comput. Phys.*, 17(1):10–18, 1975.
- [74] P. A. Maksym. Fast Monte Carlo simulation of MBE growth. *Semicond. Sci. Technol.*, 3(6):594–596, 1988.
- [75] K. A. Fichtorn and W. H. Weinberg. Theoretical foundations of dynamical Monte Carlo simulations. *J. Chem. Phys.*, 95(2):1090–1096, 1991.
- [76] M. Ahr. *Surface properties of epitaxially grown crystals*. PhD thesis, Bayerische Julius-Maximilians-Universität Würzburg, Würzburg, 2002.
- [77] J. Tersoff. Surface-Confined Alloy Formation in Immiscible Systems. *Phys. Rev. Lett.*, 74(3):434–437, 1995.
- [78] F. Liu, A. H. Li, and M. G. Lagally. Self-Assembly of Two-Dimensional Islands via Strain-Mediated Coarsening. *Phys. Rev. Lett.*, 87(12):126103, 2001.
- [79] G. E. Thayer, N. C. Bartelt, V. Ozolins, A. K. Schmid, S. Chiang, and R. Q. Hwang. Linking Surface Stress to Surface Structure: Measurement of Atomic Strain in a Surface Alloy using Scanning Tunneling Microscopy. *Phys. Rev. Lett.*, 89(3):036101, 2002.
- [80] I. Daruka and J. C. Hamilton. A two-component Frenkel-Kontorowa model for surface alloy formation. *J. Phys.: Condens. Matter*, 15(12):1827–1836, 2003.

- 
- [81] B. D. Krack, V. Ozoliņš, M. Asta, and I. Daruka. “Devil’s Staircases” in Bulk-Immiscible Ultrathin Alloy Films. *Phys. Rev. Lett.*, 88(18):186101, 2002.
- [82] Y. Ni, L. H. He, and J. Song. Strain-driven instability of a single island and a hexagonal island array on solid substrates. *Surf. Sci.*, 553(1–3):189–197, 2004.
- [83] S. Weber, M. Biehl, M. Kotrla, and W. Kinzel. Simulation of self-assembled nanopatterns in strained 2D alloys on the face centered cubic (111) surface. *J. Phys.: Condens. Matter*, 20:265004, 2008.
- [84] M. Ahr and M. Biehl. Flat (001) surfaces of ii-iv semiconductors: a lattice gas model. *Surf. Sci.*, 505:124–136, 2002.
- [85] M. Kotrla, S. Weber, F. Much, M. Biehl, and W. Kinzel. Self-organised nano-patterns in strained 2D metallic alloys: droplets vs. stripes. *Acta Metallurgica Slovaca*, 13:70–75, 2007.
- [86] J. E. Jones. On the Determination of Molecular Fields. II From the Equation of State of a Gas. *Proc. Roy. Soc.*, A106(738):463–477, 1924.
- [87] S. Zhen and G. J. Davies. Calculation of the Lennard-Jones n-m Potential Energy Parameters for Metals. *Phys. Stat. Sol. (a)*, 78(2):595–605, 1983.
- [88] R. Plass, J. A. Last, N. C. Bartelt, and G. L. Kellogg. Nanostructures: Self-assembled domain patterns. *Nature*, 412:875, 2001.
- [89] R. Plass, N. C. Bartelt, and G. L. Kellogg. Dynamic observations of nanoscale self-assembly on solid surfaces. *J. Phys.: Condens. Matter*, 14:4227–4240, 2002.
- [90] R. van Gastel, R. Plass, N. C. Bartelt, and G. L. Kellogg. Thermal Motion and Energetics of Self-Assembled Domain Structures: Pb on Cu(111). *Phys. Rev. Lett.*, 91(5):055503, 2003.
- [91] J. Tersoff. New empirical model for the structural properties of silicon. *Phys. Rev. Lett.*, 56(6):632–635, 1986.
- [92] J. Tersoff. New empirical approach for the structure and energy of covalent systems. *Phys. Rev. B*, 37(12):6991–7000, 1988.
- [93] F. Cleri and V. Rosato. Tight-binding potentials for transition metals and alloys. *Phys. Rev. B*, 48(1):22–33, 1993.
- [94] M. Schroeder. *Diffusion und Wachstum auf Kristalloberflächen*. PhD thesis, Gerhard-Mercator-Universität Duisburg, Duisburg, 1997.

- 
- [95] C. Ratsch, A. P. Seitsonen, and M. Scheffler. Strain dependence of surface diffusion: Ag on Ag(111) and Pt(111). *Phys. Rev. B*, 55(11):6750–6753, 1997.
- [96] H. Brune. Microscopic view of epitaxial metal growth: Nucleation and aggregation. *Surf. Sci. Rep.*, 31:121–229, 1998.
- [97] F. Much. Strukturbildung in der Heteroepitaxie. Diplomarbeit, Bayerische Julius-Maximilians-Universität Würzburg, Würzburg, 2000.
- [98] M. Walther. *Simulation of strain-induced and defect-controlled self-organization of nanostructures*. PhD thesis, Julius-Maximilians-Universität Würzburg, Würzburg, 2008.
- [99] J. Repp, G. Meyer, K.-H. Rieder, and P. Hyldgaard. Site Determination and Thermally Assisted Tunneling in Homogenous Nucleation. *Phys. Rev. Lett.*, 91(20):206102, 2003.
- [100] A. Götzhäuser and G. Ehrlich. Atom Movement and Binding on Surface Clusters: Pt on Pt(111) Clusters. *Phys. Rev. Lett.*, 77(7):1334–1337, 1996.
- [101] A. Losch and H. Niehus. Epitaxial growth of ultrathin Ag films on Al(111). *Surf. Sci.*, 446(1-2):153–160, 2000.
- [102] R. Stumpf and M. Scheffler. Theory of self-diffusion at and growth of Al(111). *Phys. Rev. Lett.*, 72(2):254–257, 1994.
- [103] S. C. Wang and G. Ehrlich. Self-adsorption sites on a close-packed surface: Ir on Ir(111). *Phys. Rev. Lett.*, 62(19):2297–2300, 1989.
- [104] S. C. Wang and G. Ehrlich. Atomic behavior at individual binding sites: Ir, Re, and W on Ir(111). *Phys. Rev. Lett.*, 68(8):1160–1163, 1992.
- [105] S. Papadiaz, B. Piveteau, D. Spanjaard, and M. C. Desjonquères. Structural stability of adatom islands on fcc(111) transition-metal surfaces. *Phys. Rev. B*, 54(20):14720–14727, 1996.
- [106] C. Busse, C. Polop, M. Müller, K. Albe, U. Linke, and T. Michely. Stacking-Fault Nucleation on Ir(111). *Phys. Rev. Lett.*, 91(5):056103, 2003.
- [107] A. Bogicevic, J. Strömquist, and B. I. Lundqvist. Low-Symmetry Diffusion Barriers in Homoepitaxial Growth of Al(111). *Phys. Rev. Lett.*, 81(3):637 – 640, 1998.
- [108] V. Borovikov and J. G. Amar. Mound formation and slope selection in irreversible fcc (111) growth. *Phys. Rev. B*, 72:085460, 2005.

- [109] F. H. Stillinger. Lattice sums and their phase diagram implications for the classical Lennard-Jones model. *J. Chem. Phys.*, 115(11):5208–5212, 2001.





# Danksagung

Allen, die zum Gelingen dieser Arbeit beigetragen haben, möchte ich an dieser Stelle meinen herzlichen Dank aussprechen. Insbesondere bedanke ich mich bei

- Priv. Doz. Dr. Michael Biehl für die gute Betreuung der Arbeit sowie die vielfachen Anregungen und Ideen
- Prof. Dr. Wolfgang Kinzel für die Möglichkeit, die vorliegende Arbeit an seinem Lehrstuhl anzufertigen
- Dr. Miroslav Kotrla für die Gastfreundschaft an der Tschechischen Akademie der Wissenschaften in Prag und die fruchtbare Zusammenarbeit
- Markus Walther für die hilfreichen Diskussionen und die fachliche sowie freundschaftliche Zusammenarbeit
- David Hartmann für das gründliche Korrekturlesen dieser Arbeit
- den Systembetreuern der Universität Würzburg für die gute Wartung des Computersystems
- allen Mitgliedern unseres Lehrstuhls für das freundliche und kreative Arbeitsklima
- der Deutschen Forschungsgemeinschaft für die Finanzierung dieser Arbeit
- meiner Familie für die Unterstützung während des Studiums und der Anfertigung dieser Arbeit



# Lebenslauf

## Angaben zur Person

Sebastian Weber  
geboren am 19.10.1977 in Ochsenfurt  
Staatsangehörigkeit: deutsch  
Familienstand: ledig

## Schulbildung

09/1984–07/1988 Grundschule Haßfurt  
09/1988–07/1997 Regiomontanus-Gymnasium Haßfurt,  
Allgemeine Hochschulreife

## Wehrdienst

07/1997–04/1998 Luftwaffe in Bayreuth und Neuburg/Donau

## Studium

11/1998–12/2003 Studium der Physik an der  
Bayerischen Julius-Maximilians-Universität Würzburg  
Diplomarbeit: *Hügelform und Skalenverhalten beim  
instabilen Wachstum: Ein vereinfachtes Modell*

## Promotion

01/2004–02/2008 Wissenschaftlicher Mitarbeiter am Institut für Theoretische  
Physik und Astrophysik der Universität Würzburg  
10/2006–11/2006 Forschungsaufenthalt bei Dr. Miroslav Kotrla an der  
Tschechischen Akademie der Wissenschaften in Prag

